

Multiprobe Cosmology from the Abundance of SPT Clusters and DES Galaxy Clustering and Weak Lensing

S. Bocquet¹, S. Grandis², E. Krause³, C. To^{4,5,6}, L. E. Bleem^{7,6}, M. Klein¹, J. J. Mohr^{1,8}, T. Schrabback^{2,9},
A. Alarcon^{7,10}, O. Alves¹¹, A. Amon¹², F. Andrade-Oliveira¹¹, E. J. Baxter¹³, K. Bechtol¹⁴, M. R. Becker⁷,
G. M. Bernstein¹⁵, J. Blazek¹⁶, H. Camacho^{17,18,19}, A. Campos^{20,21}, A. Carnero Rosell^{22,19,23},
M. Carrasco Kind^{24,25}, R. Cawthon²⁶, C. Chang^{5,6}, R. Chen²⁷, A. Choi²⁸, J. Cordero²⁹, M. Crocce^{30,10}, C. Davis³¹,
J. DeRose³², H. T. Diehl³³, S. Dodelson^{5,33,6}, C. Doux^{15,34}, A. Drlica-Wagner^{5,33,6}, K. Eckert¹⁵, T. F. Eifler^{3,35},
F. Elsner³⁶, J. Elvin-Poole³⁷, S. Everett³⁸, X. Fang^{39,3}, A. Ferté⁴⁰, P. Fosalba^{30,10}, O. Friedrich⁴¹, J. Frieman^{33,6},
M. Gatti¹⁵, G. Giannini^{42,6}, D. Gruen¹, R. A. Gruendl^{24,25}, I. Harrison⁴³, W. G. Hartley⁴⁴, K. Herner³³,
H. Huang^{3,45}, E. M. Huff³⁵, D. Huterer¹¹, M. Jarvis¹⁵, N. Kuropatkin³³, P.-F. Leget³¹, P. Lemos^{36,46}, A. R. Liddle⁴⁷,
N. MacCrann⁴⁸, J. McCullough^{12,31,40,1}, J. Muir⁴⁹, J. Myles¹², A. Navarro-Alsina⁵⁰, S. Pandey¹⁵, Y. Park⁵¹,
A. Porredon^{52,53}, J. Prat^{5,54}, M. Raveri⁵⁵, R. P. Rollins²⁹, A. Roodman^{31,40}, R. Rosenfeld^{56,19}, E. S. Rykoff^{31,40},
C. Sánchez¹⁵, J. Sanchez⁵⁷, L. F. Secco⁶, I. Sevilla-Noarbe⁵², E. Sheldon¹⁷, T. Shin⁵⁸, M. A. Troxel²⁷, I. Tutusaus⁵⁹,
T. N. Varga^{60,8,1}, N. Weaverdyck^{39,32}, R. H. Wechsler^{61,31,40}, H.-Y. Wu⁶², B. Yanny³³, B. Yin²⁰, Y. Zhang⁶³,
J. Zuntz⁶⁴, T. M. C. Abbott⁶³, P. A. R. Ade⁶⁵, M. Aguena¹⁹, S. Allam³³, S. W. Allen^{66,61,67}, A. J. Anderson³³,
B. Ansarinejad⁶⁸, J. E. Austermann^{69,70}, M. Bayliss⁷¹, J. A. Beall⁶⁹, A. N. Bender^{7,6,72}, B. A. Benson^{72,6,33},
F. Bianchini^{66,61,67}, M. Brodwin⁷³, D. Brooks³⁶, L. Bryant⁷⁴, D. L. Burke^{31,40}, R. E. A. Canning⁷⁵,
J. E. Carlstrom^{72,6,76,7,74}, J. Carretero⁴², F. J. Castander^{30,10}, C. L. Chang^{6,7,72}, P. Chaubal⁶⁸, H. C. Chiang^{77,78},
T.-L. Chou^{6,76}, R. Citron⁷⁹, C. Corbett Moran⁸⁰, M. Costanzi^{81,82,83}, T. M. Crawford^{6,72}, A. T. Crites⁸⁴, L. N. da
Costa¹⁹, M. E. S. Pereira⁸⁵, T. M. Davis⁸⁶, T. de Haan^{87,88}, M. A. Dobbs^{77,89}, P. Doel³⁶, W. Everett⁹⁰,
A. Farahi^{91,92}, B. Flaugher³³, A. M. Flores^{61,66}, B. Floyd⁹³, J. Gallicchio^{6,94}, E. Gaztanaga^{30,95,96}, E. M. George⁹⁷,
M. D. Gladders^{72,6}, N. Gupta⁹⁸, G. Gutierrez³³, N. W. Halverson^{90,70}, S. R. Hinton⁸⁶, J. Hlavacek-Larrondo⁹⁹,
G. P. Holder^{25,100,89}, D. L. Hollowood¹⁰¹, W. L. Holzappel¹⁰², J. D. Hrubes⁷⁹, N. Huang¹⁰², J. Hubmayr⁶⁹,
K. D. Irwin^{67,61}, D. J. James¹⁰³, F. Kéruzoré⁷, G. Khullar^{6,72}, K. Kim⁷¹, L. Knox¹⁰⁴, R. Kraft¹⁰³,
K. Kuehn^{105,106}, O. Lahav³⁶, A. T. Lee^{102,107}, S. Lee³⁵, D. Li^{69,67}, C. Lidman^{108,109}, M. Lima^{110,19}, A. Lowitz⁷²,
G. Mahler^{111,112}, A. Mantz^{66,61}, J. L. Marshall¹¹³, M. McDonald¹¹⁴, J. J. McMahon^{6,76,72}, J. Mena-Fernández¹¹⁵,
S. S. Meyer^{6,76,72,74}, R. Miquel^{116,42}, J. Montgomery⁷⁷, T. Natoli^{72,6}, J. P. Nibarger⁶⁹, G. I. Noble^{117,118},
V. Novosad¹¹⁹, R. L. C. Ogando¹²⁰, S. Padin³⁸, P. Paschos⁷⁴, S. Patil⁶⁸, A. A. Plazas Malagón^{31,40}, C. Pryke¹²¹,
C. L. Reichardt⁶⁸, J. Roberson⁷¹, A. K. Romer⁴⁶, C. Romero¹⁰³, J. E. Ruhl¹²², B. R. Saliwanchik¹²³,
L. Salvati^{124,125,126}, S. Samuroff^{16,42}, E. Sanchez⁵², B. Santiago^{127,19}, A. Sarkar¹¹⁴, A. Saro^{128,126,125,129,130},
K. K. Schaffer^{6,74,131}, K. Sharon¹³², C. Sievers⁷⁹, G. Smecher^{77,133}, M. Smith¹³⁴, T. Somboonpanyakul¹³⁵,
M. Sommer⁹, B. Stalder¹⁰³, A. A. Stark¹⁰³, J. Stephen⁷⁴, V. Strazzullo^{125,126}, E. Suchyta¹³⁶, M. E. C. Swanson²⁴,
G. Tarle¹¹, D. Thomas⁹⁵, C. Tucker⁶⁵, D. L. Tucker³³, T. Veach¹³⁷, J. D. Vieira^{25,100}, A. von der Linden⁵⁸,
G. Wang⁷, N. Whitehorn¹³⁸, W. L. K. Wu⁶⁷, V. Yefremenko⁷, M. Young¹³⁹, J. A. Zebrowski^{6,72,33}, and H. Zohren⁹
(the DES and SPT Collaborations)

(Affiliations at the end of the paper. e-mail: sebastian.bocquet@physik.lmu.de)

Cosmic shear, galaxy clustering, and the abundance of massive halos each probe the large-scale structure of the universe in complementary ways. We present cosmological constraints from the joint analysis of the three probes, building on the latest analyses of the lensing-informed abundance of clusters identified by the South Pole Telescope (SPT) and of the auto- and cross-correlation of galaxy position and weak lensing measurements (3×2pt) in the Dark Energy Survey (DES). We consider the cosmological correlation between the different tracers and we account for the systematic uncertainties that are shared between the large-scale lensing correlation functions and the small-scale lensing-based cluster mass calibration. Marginalized over the remaining Λ CDM parameters (including the sum of neutrino masses) and 52 astrophysical modeling parameters, we measure $\Omega_m = 0.300 \pm 0.017$ and $\sigma_8 = 0.797 \pm 0.026$. Compared to constraints from *Planck* primary CMB anisotropies, our constraints are only 15% wider with a probability to exceed of 0.22 (1.2 σ) for the two-parameter difference. We further obtain $S_8 \equiv \sigma_8(\Omega_m/0.3)^{0.5} = 0.796 \pm 0.013$ which is lower than the *Planck* measurement at the 1.6 σ level. The combined SPT cluster, DES 3×2pt, and *Planck* datasets mildly prefer a non-zero positive neutrino mass, with a 95% upper limit $\sum m_\nu < 0.25$ eV on the sum of neutrino masses. Assuming a w CDM model, we constrain the dark energy equation of state parameter $w = -1.15_{-0.17}^{+0.23}$ and when combining with *Planck* primary CMB anisotropies, we recover $w = -1.20_{-0.09}^{+0.15}$, a 1.7 σ difference with a cosmological constant. The precision of our results highlights the benefits of multiwavelength multiprobe cosmology and our analysis paves the way for upcoming joint analyses of next-generation datasets.

I. INTRODUCTION

The standard model of cosmology, the Lambda cold dark matter model (Λ CDM), describes the cosmic expansion history and the growth of cosmic structure and is consistent with a variety of datasets. One key pillar in testing this cosmological model is the accurate tracing of structure growth from the early universe at redshift $z \sim 1100$, when the cosmic microwave background (CMB) radiation was released, to the late-time universe $z \lesssim 2$. For over a decade, such studies have been limited by the relatively weak constraining power of late-time universe datasets, whereas primary CMB anisotropy measurements, in particular as measured by *Planck*, have exhibited tighter constraints. With the advent of wide-field lensing and galaxy surveys such as the Dark Energy Survey (DES) [1–3], the Kilo-Degree Survey (KiDS) [4], and the Hyper Suprime-Cam Subaru Strategic Program (HSC SSP) [5], however, the constraining power of local probes is boosted and is about to reach the regime where the clustering properties of matter at $z \lesssim 1$ can be determined as precisely as those at $z \sim 1100$.

A key probe of the matter power spectrum enabled by these surveys is the measurement of the three possible two-point correlation functions (hence 3×2 pt) among the galaxy position and galaxy weak lensing fields. Such measurements have provided tight cosmological constraints [6–10] with a tantalizing hint that the late-time universe may not have the exact properties as expected from interpreting the *Planck* data in the context of the Λ CDM model: The parameter S_8 tends to be somewhat low in the late-time universe constraints.¹

Another key probe of late-time structure formation on megaparsec scales is the abundance of massive halos and of the galaxy clusters they host. While clusters can be identified in optical data, a particularly robust and well-understood selection scheme consists in observing the halos’ hot intra-cluster medium, which emits X-rays via Bremsstrahlung and which causes a spectral distortion of the CMB via the thermal Sunyaev-Zel’dovich effect (hereafter SZ) [11]. High-resolution, deep millimeter-wave surveys of the CMB enabled the first blind detection of a galaxy cluster in 2009 [12] and by now have enabled the detection of thousands of massive clusters out to $z \lesssim 2$, e.g., [13–18]. To turn the abundance of SZ-selected clusters into a cosmological probe, one needs to relate the strength of the SZ signature to the underlying halo mass (we refer to this exercise as *mass calibration*). The halo mass creates the link to the halo mass function and thus the cosmological parameters and model. A particularly robust means of mass calibration is based on measurements of weak gravitational shear

around clusters, which can be modeled with exquisite control over systematic uncertainties. Indeed, the analysis of SZ-selected clusters discovered in data from the South Pole Telescope (SPT) [19] with weak-lensing mass calibration using DES and *Hubble Space Telescope* (HST) data enables competitive cosmological constraints [20]. In the $\Omega_m - \sigma_8$ parameter space, the difference of these constraints relative to the DES Year 3 (Y3) 3×2 pt results has a probability to exceed (PTE) of 0.25 (1.1σ).²

In this paper, we present a joint analysis of the abundance of SPT-selected galaxy clusters and galaxy clustering and weak lensing two-point correlation functions measured in the DES Y3 dataset. The SPT cluster mass calibration relies on weak-lensing shear profiles measured in DES Y3 data, but because these profiles are restricted to small scales $r < 3.2/(1+z_{\text{cluster}}) h^{-1} \text{Mpc}$, and because the SPT analysis is still limited by statistical uncertainties, one expects little to no correlation with the 3×2 pt measurements on larger scales. Therefore, our joint analysis enables significantly tighter constraints than obtained from the probes individually.

The first joint analysis of the abundance of *optically* selected galaxy clusters, cluster mass calibration from *large-scale* cluster lensing, cluster clustering, and cluster-galaxy clustering, and 3×2 pt [21] used data from the $1,321 \text{ deg}^2$ DES Year 1 survey. A sample of 4,794 galaxy clusters [22] was analyzed jointly with weak lensing [23, 24] and galaxy clustering [25] data, building on the DES Year 1 3×2 pt analysis [26]. The analysis presented here complements the DES Year 1 multiprobe analysis as we use a different cluster selection, mass calibration, and inference methodology.

In Section II, we review the 3×2 pt and cluster datasets and summarize the respective analysis frameworks. In Section III, we discuss the correlations between the two datasets and how we join the two analyses. We present the results in Section IV and conclude with a summary in Section V.

II. DATA AND INDIVIDUAL ANALYSIS FRAMEWORKS

We use data from the first three years of DES (covering nearly $5,000 \text{ deg}^2$) and from the first two SPT surveys (SPT-SZ and SPTpol, covering a total of nearly $5,200 \text{ deg}^2$), along with additional cluster follow-up data as described below. The two surveys share a common patch of $3,567 \text{ deg}^2$.

¹ $S_8 \equiv \sigma_8 \sqrt{\Omega_m/0.3}$ is a combination of the amplitude of fluctuations in the linear matter density field σ_8 and the matter density Ω_m . In the two-dimensional $\Omega_m - \sigma_8$ plane, S_8 is the combination that is best constrained by current cosmic shear analyses.

² The PTE is the probability of obtaining a larger difference between two measurements or between a measurement and a model prediction than what is observed. A very low PTE would thus imply that the observed difference is larger than random chance would allow given the uncertainties.

A. DES Y3 3×2pt

We use the DES Y3 3×2pt dataset and analysis as described in [7] and references therein. Briefly, the 3×2pt analysis combines weak-lensing measurement of 100 million ‘source’ galaxies [27], obtained with the METACALIBRATION algorithm [28], and positions of 10.7 million ‘lens’ galaxies with magnitude-limited selection (MAGLIM) [29]. To enable tomography, the sources are split in four redshift bins and the lenses are split in six redshift bins, of which only four are used in the analysis.

The data vector \mathbf{d} contains the three two-point correlation function measurements and shear ratio measurements on small scales between source redshift bins that share the same lens bin [30]. The corresponding theory vector \mathbf{t}_M is computed for a given model M . In this model, the non-linear matter power spectrum is computed using HALOFIT [31, 32]. Intrinsic alignment of (source) galaxies is modeled with the tidal alignment and tidal torquing (TATT) model [33], which is an extension of the non-linear linear alignment (NLA) model. The theory vector \mathbf{t}_M depends on the parameters \mathbf{p} . These include the cosmological parameters, but also 29 nuisance parameters that describe, e.g., the lens galaxy bias, the shear and photo- z calibrations, intrinsic alignment, etc.³ The likelihood \mathcal{L} is assumed to be Gaussian and we write

$$\ln \mathcal{L}(\mathbf{d}|\mathbf{p}, M) = -\frac{1}{2} \left[\mathbf{d} - \mathbf{t}_M(\mathbf{p}) \right]^T \mathbf{C}^{-1} \left[\mathbf{d} - \mathbf{t}_M(\mathbf{p}) \right] + \text{const.} \quad (1)$$

with the covariance matrix \mathbf{C} that is computed analytically [34]. We exactly follow the DES Y3 3×2pt analysis and modeling choices as published and hence defer to [7] for details.

B. SPT (SZ+pol) cluster cosmology

The SPT cluster cosmology dataset and analysis framework are described in [35]. Cluster candidates are identified by applying a matched filter to data from the SPT-SZ, SPTpol ECS, and SPTpol 500d surveys and measuring the detection significance ξ [13, 16, 36]. Over the footprint of the SPT survey that is shared with DES, we consider detections with $\xi > 4.25$ for SPTpol 500d, $\xi > 4.5$ for SPT-SZ, and $\xi > 5$ for SPTpol ECS. We perform the cluster confirmation and redshift assignment using the multi-component matched filter algorithm (MCMF) [37, 38]. We use DES data, and at high redshift $z > 1.1$, data from the Wide-field Infrared Survey Explorer (WISE) [39]. In essence, a candidate is

confirmed as a cluster if the measured richness λ exceeds a redshift-dependent limit $\lambda_{\min}(z)$ that is calibrated to ensure a target purity of $> 98\%$. Outside of the shared survey footprint, we consider detections with $\xi > 5$ and perform the cluster confirmation and redshift determination based on targeted follow-up observations (using among others, the PISCO imager [40] and *Spitzer*/IRAC [41]) as described in [13, 36].

The cosmology sample comprises 1,005 confirmed clusters at $z > 0.25$. A subset of 688 clusters at $z < 0.95$ also have DES Y3 weak-lensing data [35], and 39 clusters at higher redshifts of $0.6 - 1.7$ have weak-lensing data from HST [42–46]. The lensing measurements exclude the cluster core regions and are restricted to the well-understood small-scale 1-halo term regime. For DES, we consider scales between $0.5 h^{-1}\text{Mpc}$ and $3.2/(1+z) h^{-1}\text{Mpc}$, and for HST, scales between 0.5Mpc and 1.5Mpc . The individual radial profiles of the tangential shear \mathbf{g}_t , along with a ‘lensing mass to halo mass’ relation $M_{\text{WL}} - M_{\text{halo}}$ that accounts for all stochastic and systematic uncertainties [47], are used to calibrate the mean observable–mass relation. We describe the cluster sample and the weak-lensing data using a Bayesian hierarchical model

$$\begin{aligned} \ln \mathcal{L} \left(\{ \xi_i, \lambda_i, z_i, \mathbf{g}_{t,i} \}_{i=1}^{N_{\text{cluster}}} | \mathbf{p}, M \right) = & \\ & \sum_{i=1}^{N_{\text{cluster}}} \ln \frac{d^4 N_M(\mathbf{p})}{d\xi d\lambda d\mathbf{g}_t dz} \Big|_{\xi_i, \lambda_i, \mathbf{g}_{t,i}, z_i} \\ & - \int \dots \int d\xi d\lambda d\mathbf{g}_t dz \frac{d^4 N_M(\mathbf{p})}{d\xi d\lambda d\mathbf{g}_t dz} \Theta_s(\xi, \lambda, z) \\ & + \text{const.} \end{aligned} \quad (2)$$

with the sample selection $\Theta_s(\xi, \lambda, z)$ and where the index i runs over all clusters in the sample. The differential cluster abundance is computed as

$$\begin{aligned} \frac{d^4 N_M(\mathbf{p})}{d\xi d\lambda d\mathbf{g}_t dz} = \int d\Omega_s \int \dots \int dM d\zeta d\tilde{\lambda} dM_{\text{WL}} & \\ P(\xi|\zeta) P(\lambda|\tilde{\lambda}) P(\mathbf{g}_t | M_{\text{WL}}, \mathbf{p}) & \\ P(\zeta, \tilde{\lambda}, M_{\text{WL}} | M, z, \mathbf{p}) & \\ \frac{d^2 N(M, z, \mathbf{p})}{dM dV} \frac{d^2 V(z, \mathbf{p})}{dz d\Omega_s} & \end{aligned} \quad (3)$$

with the halo mass function [48] $\frac{d^2 N(M, z, \mathbf{p})}{dM dV}$ and the differential volume $\frac{d^2 V(z, \mathbf{p})}{dz d\Omega_s}$ within the survey footprint Ω_s . The second line in Eq. (3) contains the relationships between the observed (and thus noisy) cluster properties and the intrinsic ones. Finally, $P(\zeta, \tilde{\lambda}, M_{\text{WL}} | M, z, \mathbf{p})$ describes the multiobservable-to-mass scaling relations, including the effects of correlated intrinsic scatter. For the cluster analysis, the vector \mathbf{p} contains the cosmological parameters along with 23 parameters that describe the observable–mass relations and importantly, the systematic uncertainties in the weak-lensing modeling.

³ Note that of the 29 nuisance parameters of the DES Y3 3×2pt model, only those describing the calibration of the effective source redshift distribution and residual shear biases may be correlated with the SPT cluster lensing analysis (see Section III B).

III. ANALYSIS METHOD

In this section, we describe how we join the DES Y3 3×2pt and SPT cluster abundance analyses. We note that the two analyses were performed blindly to avoid confirmation bias. Because we strictly follow the analysis choices and modeling frameworks of the existing analyses, we do not need to (and cannot) perform a blind analysis.

We summarize our joint analysis as follows, and refer the reader to the individual subsections for further details. We compute the cross-covariance between the two datasets due to the coupling of long-range modes in the matter density field. Given the current size of the cluster sample and the current magnitude of the shot and shape noise in the cluster lensing measurements, we find that the cross-covariance does not contribute significantly and is ignored in the analysis that follows. Therefore, we can simply sum the existing log-likelihood functions [Eqs. (1) and (2)], but we account for the fact that some of the lensing systematics (in particular, the uncertainty on the source redshift distribution) are shared between the 3×2pt analysis and the cluster mass calibration. We do so by imposing a correlation between the respective parameters [see Eq. (5) below]. Instead of sampling the high-dimensional parameter space (six Λ CDM parameters, 29 nuisance parameters for 3×2pt, 23 parameters for the cluster observable–mass relations), we importance sample the respective posterior parameter distributions. To overcome the inherent noise in importance sampling, we train normalizing flows from which we can draw sufficiently large numbers of samples to obtain our final constraints. Finally, we assess the quality of the joint fit and conclude that the mean recovered model is an adequate description of the data.

A. Impact of cross-covariance between the SPT cluster abundance and DES 3×2pt

Galaxy clusters trace the peaks of the large-scale structure. Hence, the abundance of galaxy clusters and halo-scale cluster mass profiles (probed by small-scale cluster lensing) are inherently correlated with tracers of the cosmic density field. In turn, the cross-covariance of cluster and 3×2pt measurements in the same survey footprint and with overlapping redshift ranges and scales is non-zero. Note that in our analysis, however, the expected level of cross-covariance is small because the angular scales tested by the two probes are different. In this section, we demonstrate that we can safely ignore this cross-covariance given the level of uncertainties in the current measurements. Neglecting the cross-covariance has the practical advantage that no additional development for a joint analysis pipeline is needed and that we can instead keep utilizing the existing ones.

First, we verify that for the SPT dataset, the uncertainties in the cluster lensing and abundance measurements are dominated by shape and shot noises. Adopting

a halo model approach [49, 50], we analytically calculate the covariance matrix of the cluster abundance and the stacked cluster lensing data. This calculation assumes that clusters are separated into two bins in SPT detection significance ξ and three redshift bins. The cluster sample selection also involves a cut in optical richness, the so-called ‘optical cleaning’, e.g., [37, 38]. For the SPT cluster sample, the impact of optical cleaning is small, and for simplicity, we ignore it here (but we do account for it in the cluster likelihood). We generate the simulated data vector \mathbf{d}_{sim} and the covariance matrix Σ using the scale cuts for cluster lensing as in the SPT analysis [35], and assuming the best-fit ξ –mass relation and cosmological values obtained from that analysis [20]. We then calculate the signal-to-noise ratio

$$\text{SNR} \equiv \sqrt{\mathbf{d}_{\text{sim}}^T \Sigma^{-1} \mathbf{d}_{\text{sim}}} \quad (4)$$

of the simulated data with the full covariance matrix and with the covariance matrix that only contains shape and shot noise terms. We find that the signal-to-noise ratios of the two covariance matrices differ at the $\sim 3\%$ level, which would have minimal impact on the cosmological constraints. We note that the SPT cluster lensing analysis [35], and thus also this work, does not perform a stacked analysis; instead, it considers each cluster individually in a hierarchical Bayesian likelihood framework. This is equivalent to an analysis with infinitely small ξ and redshift bins. To apply our stacked result to [20], we verify the sensitivity of our calculation to the number of ξ and redshift bins. Specifically, we perform another set of stacked analyses by increasing the number of bins by a factor of six and do not see a difference in our result. We thus conclude that our result also applies to the analysis framework adopted in [20].

The fact that the cluster lensing and abundance data vectors are dominated by shot and shape noise already justifies ignoring the cross-covariance between the cluster data vector and the 3×2pt data vector in our combined analysis. However, we explicitly test the impact of ignoring this cross-covariance term on our combined analyses. Still using the halo model approach, we calculate the full covariance matrix of 3×2pt, cluster abundance, and cluster lensing. We then calculate the signal-to-noise ratio of the whole 3×2pt and cluster data vector using the full covariance matrix and using the covariance matrix without cross terms of 3×2pt and cluster parts. We find that the differences in signal-to-noise ratios are at the $\sim 0.05\%$ level, solidifying our conclusion that we can safely assume that the cluster dataset and 3×2pt are independent of each other.

B. Determination of shared systematics

As the DES weak-lensing measurements of SPT clusters and the shear two-point correlation functions that enter the DES 3×2pt data vector use the same lensing

source galaxy shapes and photo- z s, systematic uncertainties in these properties impact both cosmological probes in a correlated way. Note that there is no correlation between the DES galaxy position two-point correlation function and the SPT cluster abundance. Similarly, the 39 cluster lensing measurements based on HST data are not correlated with the DES lensing dataset. For the DES Y3 3×2 pt analysis, the lensing source galaxies were split in four tomographic bins according to their mean redshift estimates. For each bin b , a mean redshift bias Δz_s^b and a mean multiplicative shear bias m^b were determined, along with the systematic uncertainties on both quantities (eight parameters in total) [51, 52]. The SPT cluster lensing analysis used the same source selection, although tomographic bin 1 was dropped entirely [35]. The systematic uncertainty in the cluster weak-lensing mass calibration was determined by calibrating a ‘weak-lensing mass to halo mass’ relation ($M_{\text{WL}} - M_{\text{halo}}$, see Eqs. (36)–(38) in [35]) using Monte Carlo simulations of synthetic cluster lensing measurements based on mass maps from hydrodynamical simulations (following [47]). In these Monte Carlo simulations, the lensing source photo- z s and the shear bias parameters m were stochastically drawn from the calibrated distributions, thereby incorporating the effects of the uncertain photo- z and shear calibration into the uncertainties in the $M_{\text{WL}} - M_{\text{halo}}$ relation.

In this work, we repeat the calibration of the cluster lensing model, but for each Monte Carlo realization, we now also record the shear bias m^b and the uncertainty on the mean redshift Δz_s^b for each tomographic bin b . This allows us to track the correlation between the parameters of the $M_{\text{WL}} - M_{\text{halo}}$ model and Δz_s^b and m^b . We determine that only the first principal component of the cluster weak-lensing mass bias b_{WL} and the mean redshift bias of the 4th tomographic redshift bin Δz_s^4 (anti)correlate significantly, with a correlation coefficient $\rho = -0.81$.⁴ The negative correlation is explained as follows: If, for example, the source redshift is biased low, then, for a given lensing signal, the inferred lensing mass would be biased high, and with it, the amplitude of the $M_{\text{WL}} - M_{\text{halo}}$ relation. All other parameters exhibit negligible levels of correlation. This is expected because only at relatively large cluster redshifts does the uncertainty in the photo- z calibration represent a significant contribution to the overall systematic error budget (see discussion and Fig. 10 in [35]). The uncertainty in the shear calibration is negligible at all cluster redshifts. In our analysis, we account for the correlation ρ as discussed in the next subsection.

We note that the characterization of the shared systematics between 3×2 pt and the weak-lensing cluster mass calibration as performed here is straightforward because of the deliberate choice taken in the SPT cluster

cosmology analysis to perform the cluster weak-lensing analysis based on the same source selection as used for the DES lensing two-point correlation functions. While alternative, more optimal cluster lensing source selection schemes would almost certainly have led to slightly reduced statistical uncertainties, the characterization of the systematic uncertainties, and in particular the characterization of their correlation with the systematic uncertainties in 3×2 pt would have been more complicated. Therefore, we recommend a similar analysis philosophy also for future multiprobe analyses that include weak-lensing calibrated cluster abundance measurements.

C. Parameter inference

We follow the DES Y3 3×2 pt analysis and apply the same uniform priors on Ω_m , Ω_b , $\Omega_\nu h^2$, h , n_s , and A_s , see Table I in [7]. We consider σ_8 as a derived parameter.

As demonstrated in the previous subsections, the cluster abundance and mass calibration likelihood and the 3×2 pt likelihood are effectively independent. Therefore, instead of running an excessively expensive MCMC chain to explore the joint high-dimensional parameter space, we adopt an importance sampling approach. In this approach, the samples of the posterior parameter distribution of one analysis get updated weights corresponding to the likelihood of the other analysis. Typically though, this procedure leads to noisy posterior distributions because the effective sample size decreases. To mitigate this effect, we first train normalizing flows to learn the posterior distributions of the SPT cluster and DES 3×2 pt analyses.⁵

A normalizing flow is a generative model in machine learning that learns the bijective mapping between a simple distribution and the target probability distribution [53–55]. In our case, the simple distribution is a multivariate normal distribution, and the training set is the samples of an MCMC chain (from the SPT or DES analysis). Once the transformation is known, one can draw a large number of samples from the target distribution by drawing samples from the normal distribution and applying the transformation. Furthermore, one can obtain the posterior probability at any point in parameter space by applying the inverse transformation. We use a modified implementation of FLOWJAX⁶ that can handle weighted samples.⁷

In this work, we are interested in the improvements on the cosmological parameter constraints enabled by the

⁴ Note that the first principal component of the cluster lensing mass bias is defined as $\sigma_{\ln b_{\text{WL},1}}$ in the SPT analysis [20, 35] but we use a shorter notation b_{WL} here.

⁵ The original SPT cluster analysis assumed different priors on the cosmological parameters [20]. To enable the importance sampling analysis, we reran the cluster analysis using the DES Y3 priors. The recovered results were essentially unchanged.

⁶ <https://danielward27.github.io/flowjax>

⁷ Our implementation is available at <https://github.com/SebastianBocquet/flowjax>.

joint analysis. Therefore, we restrict the importance sampling to the parameters Ω_m , Ω_b , $\Omega_\nu h^2$, h , n_s , σ_8 , and the correlated nuisance parameters b_{WL} and Δz_s^4 . This reduces the dimensionality of the parameter space to eight and improves the stability of the normalizing flows and of the importance sampling analysis. In the Appendix, we demonstrate that the trained flows are able to accurately reproduce the true distributions (see the upper-right triangle in Fig. 6). We now draw a large number of samples from one flow, and update the sample weights w using the likelihood at that location in parameter space from the other flow. Finally, we account for the correlation between b_{WL} and Δz_s^4 (see previous section) by updating the sample weights

$$\begin{aligned} \boldsymbol{\delta} &\equiv \begin{pmatrix} b_{\text{WL}} - \langle b_{\text{WL}} \rangle \\ \Delta z_s^4 - \langle \Delta z_s^4 \rangle \end{pmatrix}, \\ \boldsymbol{\Sigma}_{\text{uncorr.}} &\equiv \begin{pmatrix} \sigma_{b_{\text{WL}}}^2 & 0 \\ 0 & \sigma_{\Delta z_s^4}^2 \end{pmatrix}, \\ \boldsymbol{\Sigma}_{\text{corr.}} &\equiv \begin{pmatrix} \sigma_{b_{\text{WL}}}^2 & \rho \sigma_{b_{\text{WL}}} \sigma_{\Delta z_s^4} \\ \rho \sigma_{b_{\text{WL}}} \sigma_{\Delta z_s^4} & \sigma_{\Delta z_s^4}^2 \end{pmatrix}, \\ \ln w_{\text{with corr.}} &= \ln w_{\text{no corr.}} + \frac{1}{2} \boldsymbol{\delta}^T \boldsymbol{\Sigma}_{\text{uncorr.}}^{-1} \boldsymbol{\delta} - \frac{1}{2} \boldsymbol{\delta}^T \boldsymbol{\Sigma}_{\text{corr.}}^{-1} \boldsymbol{\delta}. \end{aligned} \quad (5)$$

We use the importance sampled chains to extract the parameter constraints presented in this work. Our baseline results are based on the DES Y3 3×2pt chain, updated with the SPT cluster likelihood and after applying Eq. (5). These constraints are shown in solid red in Fig. 6. To cross-check that the importance sampling scheme is robust, we also extract results starting from the SPT cluster chain, importance sampling using the DES Y3 3×2pt likelihood, and applying Eq. (5), as shown in red dashed in Fig. 6. The two analysis routes lead to almost indistinguishable results, confirming the reliability of our approach.

D. Goodness of fit

We test whether the best-fit model for the joint cluster and 3×2pt analysis is an adequate description of the data. The 3×2pt data vector contains 471 data points. The χ^2 at the maximum a posteriori probability (MAP) of the joint analysis ($\chi^2 = 538.5$) is higher than the χ^2 at the MAP of the 3×2pt Λ CDM analysis by $\Delta\chi^2 = 1.8$. Note that if the MAP of the joint analysis is not identical to the MAP of the individual probe (and if the priors are not changed) then a somewhat worse fit is to be expected by definition. The 3×2pt analysis does not show signs of significant internal inconsistencies (PTE of 0.023 [7, 56]). Because the increase in χ^2 we observe is not large given the number of data points, we conclude that the 3×2pt data is well fit in our joint analysis, too. We also compare the total number of clusters and the measured stacked shear profiles with the model predictions at the MAP of

the joint analysis (analogous to Figs. 1 and 2 in [20]) and obtain $\chi^2 = 43.1$ for 27 data points, with a corresponding PTE of 0.03 ($\chi^2 = 35.6$ for the clusters-only analysis). Note that the cluster analysis is performed using an unbinned Poisson likelihood for the cluster sample and a hierarchical Bayesian likelihood for the individual cluster lensing shear profiles. Stacked data are only used to evaluate the goodness of fit. We conclude that the model is an adequate description of the joint dataset and present the recovered cosmological constraints.

IV. RESULTS

We present our constraints on Λ CDM, the sum of neutrino masses, and w CDM. Throughout this work, we assume spatial flatness and a uniform prior [0.06, 0.6] eV for the sum of neutrino masses (the lower limit is given by measurements of neutrino oscillations, see e.g., [57]).

A. Λ CDM

Figure 1 (left) shows Λ CDM constraints in the $\Omega_m - \sigma_8$ plane as obtained by SPT clusters, DES 3×2pt, and our joint analysis SPT clusters + DES 3×2pt. The constraints on a selection of parameters are presented in Table I. The joint constraints lie at the intersection of the two individual probes. The degeneracy direction mostly follows the degeneracy of the 3×2pt result; the parameter combination that is constrained with the smallest absolute uncertainty is $\sigma_8(\Omega_m/0.3)^{0.494}$, which is essentially S_8 . The ratio of the areas of the 95% credible region in $\Omega_m - \sigma_8$ space for SPT clusters, DES 3×2pt, and the joint analysis is 3.3 : 2.1 : 1. While the two probes cannot individually constrain the Hubble constant, the joint analysis breaks some of the parameter degeneracies and we recover $h = 0.73 \pm 0.07$ (see also Fig. 6 in the Appendix). However, this result is not strong enough to inform the Hubble tension.

In the $\Omega_m - \sigma_8$ plane shown in Fig. 1, the 95% credible region of the SPT cluster + DES 3×2pt analysis is 15% larger than for *Planck* 2018 TT,TE,EE+lowE [58]. We quantify the two-parameter difference with a PTE of 0.22 (1.2 σ). Our measurement $S_8 = 0.796 \pm 0.013$ differs from the *Planck* measurement $S_8 = 0.831 \pm 0.017$ at 1.6 σ . We show lines of constant S_8 in the figure to help guide the eye. Because the difference is not significant, we combine our joint constraints with *Planck* temperature and polarization power spectra to obtain tight constraints on the cosmological parameters. In Fig. 1 (right), we also show the results from the multiprobe analyses of DES Y1 cluster abundance, cluster clustering, galaxy clustering, and lensing [21] and of CMB lensing measured by the Atacama Cosmology Telescope (ACT) and baryon acoustic oscillations (BAO) measured in the 6dF and SDSS galaxy surveys [59, 60]. In the $\Omega_m - \sigma_8$ plane, the ratio of the areas of the 95% credible regions of the DES Y1, ACT

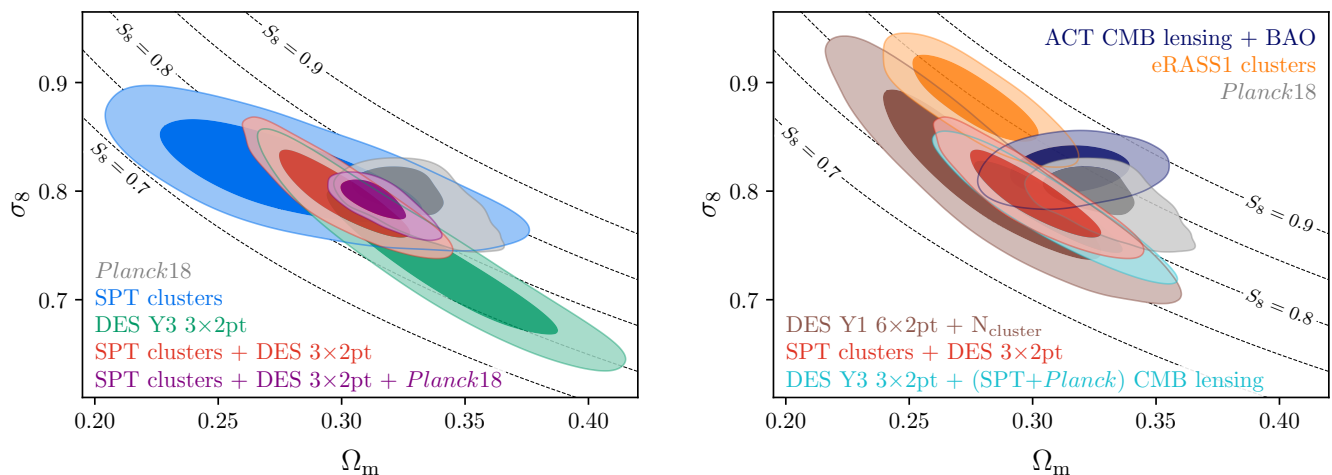


FIG. 1. Constraints on Ω_m and σ_8 (68% and 95% credibility) in Λ CDM with massive neutrinos. The two panels show the same parameter ranges. Dashed lines show lines of constant $S_8 \equiv \sigma_8 \sqrt{\Omega_m}/0.3$. *Left panel:* The individual lensing-informed SPT cluster abundance and DES 3 \times 2pt results, along with their combination. We also show the constraints from *Planck*18 TT,TE,EE+lowE primary CMB anisotropies and the combination with our joint analysis. *Right panel:* Comparison of our SPT clusters + DES 3 \times 2pt results with a selection of external single-probe and multiprobe analyses.

+ BAO, and our SPT clusters + DES 3 \times 2pt analyses is 2.8 : 1.0 : 1. Our results are similar to the joint analysis of DES Y3 galaxy clustering and lensing and SPT+*Planck* CMB lensing [61], but somewhat tighter.

Comparing to the eROSITA eRASS1 cluster cosmology analysis [62], if we assume that their analysis is independent from ours, we find that their reported value of σ_8 is higher than ours at the 2.4σ level, and we find a PTE of 0.018 (2.4σ) in the Ω_m - σ_8 plane. In reality, however, the footprints of the DES, SPT, and eRASS1 surveys overlap and the eRASS1 and SPT cluster samples have objects in common, and both analyses rely on mass calibration using DES lensing data [35, 63]. Carefully assessing the statistical significance of the difference is not the main goal of this study, and we leave this quantification for future works.

B. Sum of neutrino masses

Following the DES 3 \times 2pt analysis, we set a lower limit $\sum m_\nu > 0.06$ eV to reflect constraints from neutrino oscillations. Measurements of *Planck*18 TT,TE,EE+lowE primary CMB anisotropies place an upper limit $\sum m_\nu < 0.30$ eV at 95% credibility [58]. As shown with the gray contours in Fig. 2, this constraint is limited by degeneracies with Ω_m , σ_8 , and h . Therefore, the combination of CMB data with independent measurements of these other cosmological parameters breaks (some of) these degeneracies and enables tighter constraints. In Fig. 2, we show that while our joint SPT clusters + DES 3 \times 2pt analysis cannot meaningfully constrain $\sum m_\nu$, it breaks the degeneracies with Ω_m and σ_8 in the CMB analysis. In Fig. 3, we show the marginalized posterior probability

distribution for the sum of neutrino masses. The constraints from *Planck*18 and from the combination of that dataset with either 3 \times 2pt or the SPT cluster abundance peak at the minimum allowed mass. However, the upper limits in all three analyses cannot rule out the inverted hierarchy, which would imply $\sum m_\nu > 0.1$ eV. Interestingly, due to the breaking of degeneracies in the non-trivial high-dimensional parameter space, the combination of *Planck*18 and our joint SPT clusters + DES 3 \times 2pt analysis results in a constraint on the sum of neutrino masses that peaks at a non-zero value of 0.09 eV (mean value is 0.14 eV, see also Table I). However, the credible intervals are still wide enough that both the normal and the inverted mass hierarchy are compatible with our results.

For comparison, in Fig. 2, we also show the combination of CMB and BAO data from the Dark Energy Spectroscopic Instrument (DESI) [64]. While BAO do not constrain σ_8 , they provide measurements on Ω_m and h and thus break the degeneracies in the CMB analysis (see also, e.g., [65]) in a way that is complementary to our SPT clusters + DES 3 \times 2pt analysis.

C. w CDM

We now additionally allow the dark energy equation of state parameter w to vary. Figure 4 shows the constraints from DES 3 \times 2pt, from the SPT cluster abundance, and from our joint analysis. The constraints on Ω_m and σ_8 are comparable with the constraints recovered for the Λ CDM model. We report $w = -1.15^{+0.23}_{-0.17}$, which improves over the single-probe uncertainties by 35 and 22%, and which agrees with a cosmological constant

TABLE I. Parameter constraints for the Λ CDM and w CDM models, marginalized over all cosmology and 52 nuisance parameters (mean and 68% credible intervals, or 95% limit). $\sigma_8 (\Omega_m/0.3)^{0.5}$ is the parameter combination that is best constrained by 3×2 pt, and $\sigma_8 (\Omega_m/0.3)^{0.25}$ is the combination that is best constrained by the SPT cluster abundance. The cluster and 3×2 pt datasets cannot individually constrain h and we only quote the joint constraint (but we always marginalize over h). The joint analysis does not meaningfully constrain $\sum m_\nu$ on its own, and we only quote the constraint obtained in combination with *Planck* 2018 TT,TE,EE+lowE. Note that while the w CDM constraints from SPT clusters only are affected by the hard prior $w > -2$, the contours of the joint constraints close.

Dataset	Ω_m	σ_8	$S_8 \equiv \sigma_8 (\frac{\Omega_m}{0.3})^{0.5}$	$\sigma_8 (\frac{\Omega_m}{0.3})^{0.25}$	h	$\sum m_\nu$ [eV]	w
ΛCDM							
SPT clusters	0.286 ± 0.032	0.817 ± 0.026	0.795 ± 0.029	0.805 ± 0.016	-1
DES 3×2 pt	$0.339^{+0.032}_{-0.031}$	$0.733^{+0.039}_{-0.049}$	0.776 ± 0.017	0.754 ± 0.031	-1
SPT clusters + DES 3×2 pt	0.300 ± 0.017	0.797 ± 0.026	0.796 ± 0.013	0.796 ± 0.017	0.73 ± 0.07	...	-1
SPT clusters + DES 3×2 pt + <i>Planck</i>	0.314 ± 0.009	0.791 ± 0.013	0.809 ± 0.009	0.800 ± 0.010	0.674 ± 0.007	$0.14^{+0.02}_{-0.07} (< 0.25)$	-1
wCDM							
SPT clusters	0.268 ± 0.037	0.820 ± 0.026	0.772 ± 0.040	0.796 ± 0.020	-1.45 ± 0.31
DES 3×2 pt	$0.352^{+0.035}_{-0.041}$	$0.719^{+0.037}_{-0.044}$	$0.775^{+0.026}_{-0.024}$	0.746 ± 0.029	$-0.98^{+0.32}_{-0.20}$
SPT clusters + DES 3×2 pt	0.294 ± 0.021	0.793 ± 0.023	0.784 ± 0.019	0.788 ± 0.015	0.71 ± 0.06	...	$-1.15^{+0.23}_{-0.17}$
SPT clusters + DES 3×2 pt + <i>Planck</i>	0.284 ± 0.018	0.811 ± 0.020	0.787 ± 0.016	0.799 ± 0.013	0.715 ± 0.024	$0.25^{+0.07}_{-0.19} (< 0.50)$	$-1.20^{+0.15}_{-0.09}$

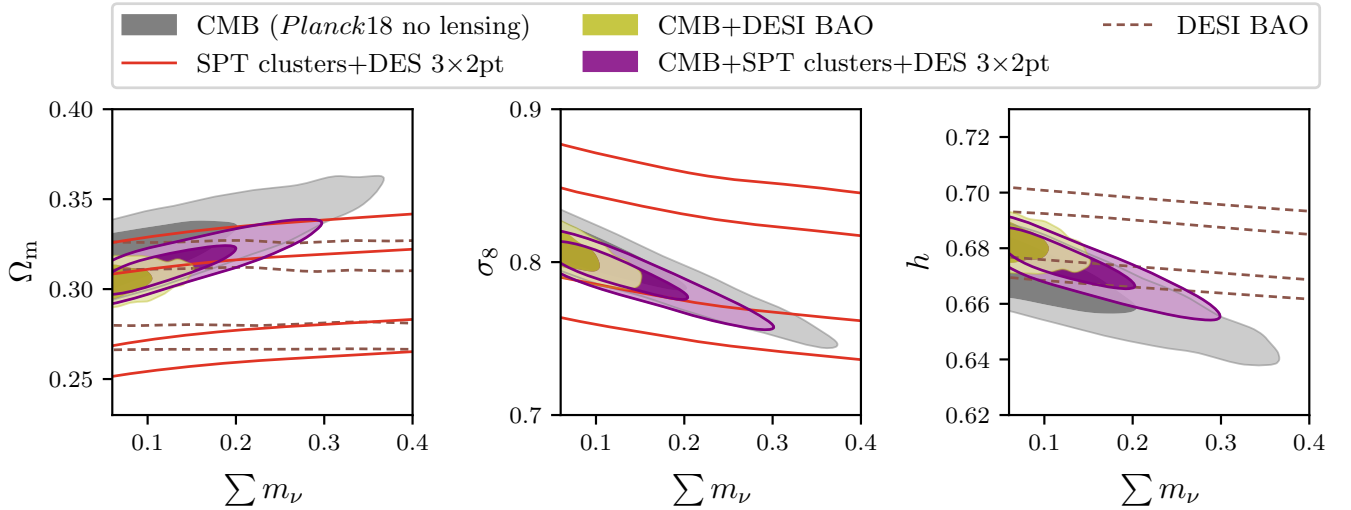


FIG. 2. Joint constraints on the sum of neutrino masses $\sum m_\nu$ and a selection of other cosmological parameters. For the sake of readability, we omit the comparatively weak constraints on h from the SPT clusters + DES 3×2 pt analysis, and we note that the BAO data do not constrain σ_8 . Neither the BAO data nor the joint SPT clusters + DES 3×2 pt analysis can meaningfully constrain $\sum m_\nu$ on their own. However, their combination with CMB data allows for refined constraints compared to those obtained from CMB data alone by breaking the $\sum m_\nu$ - Ω_m degeneracy in the CMB-based constraints. The BAO data also break the $\sum m_\nu$ - h degeneracy, while the SPT clusters + DES 3×2 pt analysis also breaks the $\sum m_\nu$ - σ_8 degeneracy.

$w = -1$ with a PTE of 0.58 (0.6σ). For reference, the purely geometrical measurement using DES Supernovae is yet another 26% tighter and peaks at a less negative value $w = -0.80^{+0.14}_{-0.16}$. The DESI BAO measurement is also purely geometric and yields $w = -0.99^{+0.15}_{-0.13}$, which is 31% tighter than our measurement and almost perfectly

centered on $w = -1$ [64]. Conversely, the results from *Planck* data alone exhibit extended degeneracies between w and many other parameters. By combining *Planck* temperature and polarization data with our SPT cluster + DES 3×2 pt dataset, we can break these degeneracies and recover tight constraints; notably, our measurement

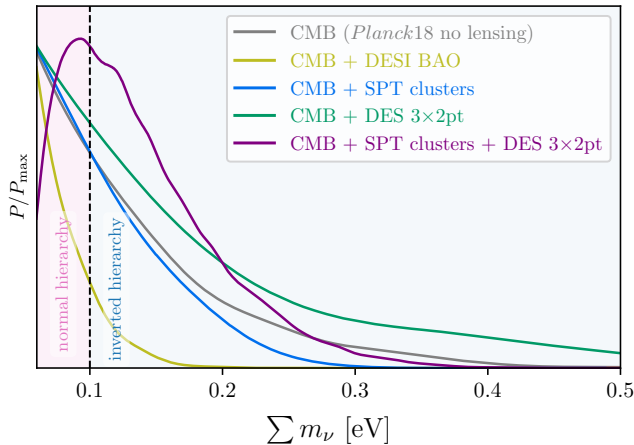


FIG. 3. Marginalized constraints on the sum of neutrino masses. For the normal hierarchy, the minimal value is $\sum m_\nu > 0.06$ eV, which is the prior we adopt in our analysis. For the inverted hierarchy, $\sum m_\nu > 0.1$ eV, as indicated by the dashed line. The posterior of the joint *Planck* + SPT clusters + DES 3×2pt analysis peaks at 0.09 eV, with no significant preference for either hierarchy.

$w = -1.20^{+0.15}_{-0.09}$ differs from a cosmological constant with a PTE of 0.09, or 1.7σ (see Table I and purple contours in Fig. 4).

The *Planck* 2018 data are known to exhibit more smoothing at high multipoles than can be explained by lensing, and this can impact the recovered parameter constraints [58]. We investigate this effect by also allowing the amplitude of CMB lensing A_L to vary, and we recover $A_L = 1.20 \pm 0.06$ and $w = -1.16^{+0.16}_{-0.10}$. The difference with a cosmological constant thus reduces to the 1σ level but A_L is greater than unity at more than 3σ .

While dark energy with a time-evolving equation of state has seen renewed interest, we do not consider this model here. Constraints on w_0 and w_a were presented using the DES Y3 3×2pt data [66] and their combination with DES Supernovae and SDSS BAO [67]. However, the SPT collaboration has not yet presented a $w_0 w_a$ CDM analysis using its cluster sample. Therefore, we leave a joint SPT clusters and DES 3×2pt analysis of the $w_0 w_a$ CDM model to future work that will show whether the contours in $w_0 - w_a$ space close, which would enable an independent cross-check of the Supernovae + BAO (+ CMB) constraints [64, 67–69].

V. SUMMARY

In this work, we present a joint analysis of weak lensing and galaxy clustering measurements from DES data and the abundance of SPT-selected clusters with DES and HST weak-lensing mass calibration. The two individual probes have roughly comparable constraining power and we show that their cosmological correlation and the cor-

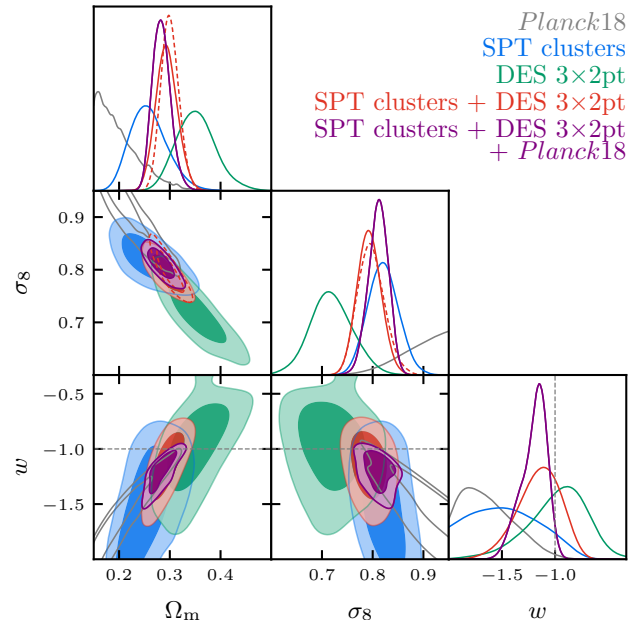


FIG. 4. Constraints on the matter density, the amplitude of fluctuations, and the dark energy equation of state parameter (68% and 95% credibility) in w CDM with massive neutrinos. For reference, we also show the Λ CDM ($w = -1$) constraints on Ω_m and σ_8 from our SPT clusters + DES 3×2pt analysis with dashed lines.

relation due to using the same DES lensing dataset are both negligible. Therefore, the joint analysis of these two probes is particularly appealing.

For a flat Λ CDM model with massive neutrinos, we report competitive constraints on Ω_m and σ_8 (see Table I). In the two-parameter plane, the 95% credibility region is only 15% larger than the one allowed by *Planck* 2018 primary CMB data (TT,TE,EE+lowE) [58]. We are thus witnessing the beginning of an era where measurements of the large-scale structure are (at least) as constraining as early-universe CMB observations. Our analysis does not provide a strong suggestion for S_8 being lower than measured by *Planck*, but as with many other published results, our measurement lies below the *Planck* value (at the 1.7σ level in our case).

The combined SPT cluster, DES 3×2pt, and *Planck* dataset shows a mild preference for a non-zero positive sum of neutrino masses with an upper limit $\sum m_\nu < 0.25$ eV. Our joint analysis improves the constraints on the dark energy equation of state parameter w over the results from the individual probes. We recover $w = -1.15^{+0.23}_{-0.17}$ from SPT clusters + DES 3×2pt, and for the joint analysis with *Planck*, $w = -1.20^{+0.15}_{-0.09}$. However, these results cannot rival the existing constraints enabled by geometric probes such as BAO and Supernovae.

This work presents the second joint analysis of the cluster abundance and 3×2pt measurements. Compared to the first analysis [21], which used optically selected clus-

ters and large-scale cluster–shear correlation functions, we use the SZ-selected SPT cluster sample and cluster lensing measurements in the small-scale, 1-halo term regime. Therefore, our analysis is complementary to the existing work. Our work paves the way for future joint analyses of larger SZ-selected cluster samples (from, e.g., SPT-3G [70], ACT [15, 17], the Simons Observatory [71], and CMB-S4 [72]), improved lensing and galaxy clustering datasets (e.g., DES Year 6, *Euclid* [73, 74], and LSST [75] obtained with the Vera C. Rubin Observatory), and updated CMB lensing measurements (such as presented in, e.g., [76]).

In these future analyses, the statistical uncertainties in the cluster abundance and cluster lensing measurements will be reduced and we expect the correlation due to using the same lensing data as 3×2 pt to no longer be negligible. The upcoming cluster sample will extend down to lower halo masses, implying that the sample (co-)variance and the cross-covariance with 3×2 pt and other large-scale structure probes might no longer be negligible, either. Our work thus sets the stage for future, more complex analyses of joint probes that will enable us to probe the large-scale structure of the universe with unprecedented constraining power.

ACKNOWLEDGMENTS

This research was supported by the Ludwig-Maximilians-Universität München, the MPG Faculty Fellowship program, and the Excellence Cluster ORIGINS, which is funded by the Deutsche Forschungsgemeinschaft (DFG, German Research Foundation) under Germany’s Excellence Strategy - EXC-2094-390783311. The Innsbruck authors acknowledge support from the Austrian Research Promotion Agency (FFG) and the Federal Ministry of the Republic of Austria for Climate Action, Environment, Mobility, Innovation and Technology (BMK) via grants 899537 and 900565, and 911971. EK is supported in part by Department of Energy grant DE-SC0020247 and the David and Lucile Packard Foundation. CT is supported by the Eric and Wendy Schmidt AI in Science Postdoctoral Fellowship, a Schmidt Futures program. Work at Argonne National Laboratory was supported by the U.S. Department of Energy, Office of High Energy Physics, under Contract No. DE-AC02-06CH11357.

The South Pole Telescope program is supported by the National Science Foundation (NSF) through awards OPP-1852617 and OPP-2332483. Partial support is also provided by the Kavli Institute of Cosmological Physics at the University of Chicago.

Funding for the DES Projects has been provided by the U.S. Department of Energy, the U.S. National Science Foundation, the Ministry of Science and Education of Spain, the Science and Technology Facilities Council of the United Kingdom, the Higher Education Funding Council for England, the National Center for Super-

computing Applications at the University of Illinois at Urbana-Champaign, the Kavli Institute of Cosmological Physics at the University of Chicago, the Center for Cosmology and Astro-Particle Physics at the Ohio State University, the Mitchell Institute for Fundamental Physics and Astronomy at Texas A&M University, Financiadora de Estudos e Projetos, Fundação Carlos Chagas Filho de Amparo à Pesquisa do Estado do Rio de Janeiro, Conselho Nacional de Desenvolvimento Científico e Tecnológico and the Ministério da Ciência, Tecnologia e Inovação, the Deutsche Forschungsgemeinschaft and the Collaborating Institutions in the Dark Energy Survey.

The Collaborating Institutions are Argonne National Laboratory, the University of California at Santa Cruz, the University of Cambridge, Centro de Investigaciones Energéticas, Medioambientales y Tecnológicas-Madrid, the University of Chicago, University College London, the DES-Brazil Consortium, the University of Edinburgh, the Eidgenössische Technische Hochschule (ETH) Zürich, Fermi National Accelerator Laboratory, the University of Illinois at Urbana-Champaign, the Institut de Ciències de l’Espai (IEEC/CSIC), the Institut de Física d’Altes Energies, Lawrence Berkeley National Laboratory, the Ludwig-Maximilians-Universität München and the associated Excellence Cluster ORIGINS, the University of Michigan, NSF’s NOIRLab, the University of Nottingham, The Ohio State University, the University of Pennsylvania, the University of Portsmouth, SLAC National Accelerator Laboratory, Stanford University, the University of Sussex, Texas A&M University, and the OzDES Membership Consortium.

Based in part on observations at Cerro Tololo Inter-American Observatory at NSF’s NOIRLab (NOIRLab Prop. ID 2012B-0001; PI: J. Frieman), which is managed by the Association of Universities for Research in Astronomy (AURA) under a cooperative agreement with the National Science Foundation.

The DES data management system is supported by the National Science Foundation under Grant Numbers AST-1138766 and AST-1536171. The DES participants from Spanish institutions are partially supported by MICINN under grants ESP2017-89838, PGC2018-094773, PGC2018-102021, SEV-2016-0588, SEV-2016-0597, and MDM-2015-0509, some of which include ERDF funds from the European Union. IFAE is partially funded by the CERCA program of the Generalitat de Catalunya. Research leading to these results has received funding from the European Research Council under the European Union’s Seventh Framework Program (FP7/2007-2013) including ERC grant agreements 240672, 291329, and 306478. We acknowledge support from the Brazilian Instituto Nacional de Ciência e Tecnologia (INCT) do e-Universo (CNPq grant 465376/2014-2).

This manuscript has been authored by Fermi Research Alliance, LLC under Contract No. DE-AC02-07CH11359 with the U.S. Department of Energy, Office of Science, Office of High Energy Physics. This research has made use of the SAO/NASA Astrophysics Data System and of

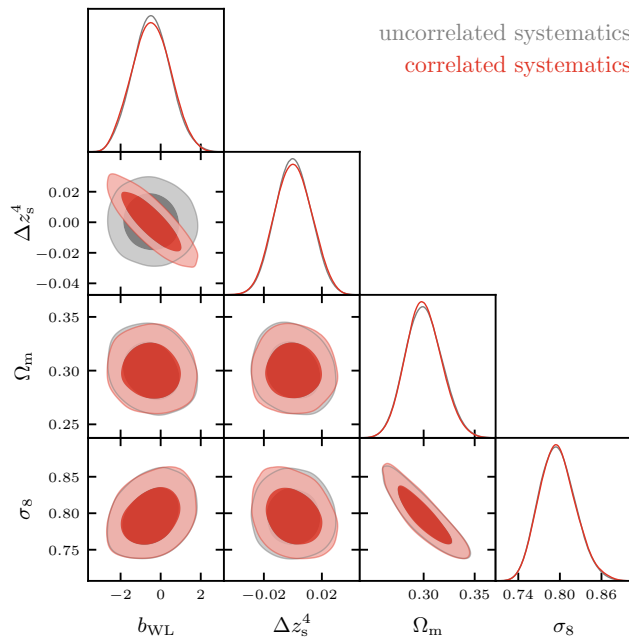


FIG. 5. Impact of the shared systematics in the lensing source photo- z calibration, which introduces a correlation $\rho = -0.81$ between the amplitude of the cluster lensing mass-to-halo mass b_{WL} and the uncertainty on the mean redshift of the lensing tomographic bin 4, Δz_s^4 . We show the 68% and 95% credibility regions. Neglecting the fact that the lensing systematics are shared between the two analyses (gray) has a negligible impact on the recovered cosmological constraints. Throughout this work, we nonetheless correctly account for the correlation (red).

ADSTEX.⁸

Appendix A: Impact of shared systematics

In our baseline analysis, we account for the correlation $\rho = -0.81$ between (one of) the parameters of the

cluster lensing mass bias b_{WL} and the mean redshift bias of the 4th tomographic bin Δz_s^4 . Here, we investigate the impact of this correlation. In Fig. 5, we show the two parameters along with the cosmological parameters of prime interest, Ω_m and σ_8 . In the baseline analysis, the correlation between the two non-cosmology parameters can be clearly seen. For comparison, we also produce constraints without accounting for the correlation of lensing systematics, which we do by not applying Eq. (5). As can be seen in the figure, ignoring the correlation between b_{WL} and Δz_s^4 has a negligible impact on the recovered cosmological constraints. This is expected, because the analyses of the individual probes are not limited by the uncertainty in the photo- z calibration. Nevertheless, in our baseline analysis, we properly take the correlation into account.

Appendix B: Robustness of Normalizing Flows and Importance Sampling

In Fig. 6, we show the SPT cluster and DES 3×2 pt chains, along with the posterior distributions obtained from the trained normalizing flows. We observe that the well-constrained parameters such as the nuisance parameters and Ω_m and σ_8 are very well reproduced by the normalizing flows, whereas the reconstruction of the other parameters seems to be more challenging. In the same figure, we also show our fiducial results, as obtained by importance sampling the 3×2 pt results with the cluster likelihood (solid red lines and contours). Finally, we also show the results obtained from the inverse approach, where we importance sample the probability distribution obtained from the cluster analysis with the 3×2 pt likelihood (dashed red lines and contours). There is very good qualitative agreement between the two sets of results, and we thus conclude that our inference scheme is robust.

-
- [1] B. Flaugher, H. T. Diehl, K. Honscheid, T. M. C. Abbott, O. Alvarez, R. Angstadt, J. T. Annis, M. Antonik, O. Ballester, L. Beaufore, et al., *AJ* **150**, 150 (2015), [arXiv:1504.02900](https://arxiv.org/abs/1504.02900).
- [2] DES Collaboration, T. Abbott, F. B. Abdalla, J. Aleksić, S. Allam, A. Amara, D. Bacon, E. Balbinot, M. Banerji, K. Bechtol, et al., *MNRAS* **460**, 1270 (2016), [arXiv:1601.00329](https://arxiv.org/abs/1601.00329).
- [3] DES Collaboration, T. M. C. Abbott, F. B. Abdalla, S. Allam, A. Amara, J. Annis, J. Asorey, S. Avila,

O. Ballester, M. Banerji, et al., *ApJS* **239**, 18 (2018), [arXiv:1801.03181](https://arxiv.org/abs/1801.03181).

- [4] J. T. A. de Jong, G. A. Verdoes Kleijn, K. H. Kuijken, and E. A. Valentijn, *Experimental Astronomy* **35**, 25 (2013), [arXiv:1206.1254](https://arxiv.org/abs/1206.1254).
- [5] H. Aihara, N. Arimoto, R. Armstrong, S. Arnouts, N. A. Bahcall, S. Bickerton, J. Bosch, K. Bundy, P. L. Capak, J. H. H. Chan, et al., *PASJ* **70**, S4 (2018), [arXiv:1704.05858](https://arxiv.org/abs/1704.05858).
- [6] C. Heymans, T. Tröster, M. Asgari, C. Blake, H. Hildebrandt, B. Joachimi, K. Kuijken, C.-A. Lin, A. G. Sánchez, J. L. van den Busch, et al., *A&A* **646**, A140 (2021), [arXiv:2007.15632](https://arxiv.org/abs/2007.15632).
- [7] DES Collaboration, T. M. C. Abbott, M. Aguena, A. Alarcon, S. Allam, O. Alves, A. Amon, F. Andrade-

⁸ <https://github.com/yymao/adstex>

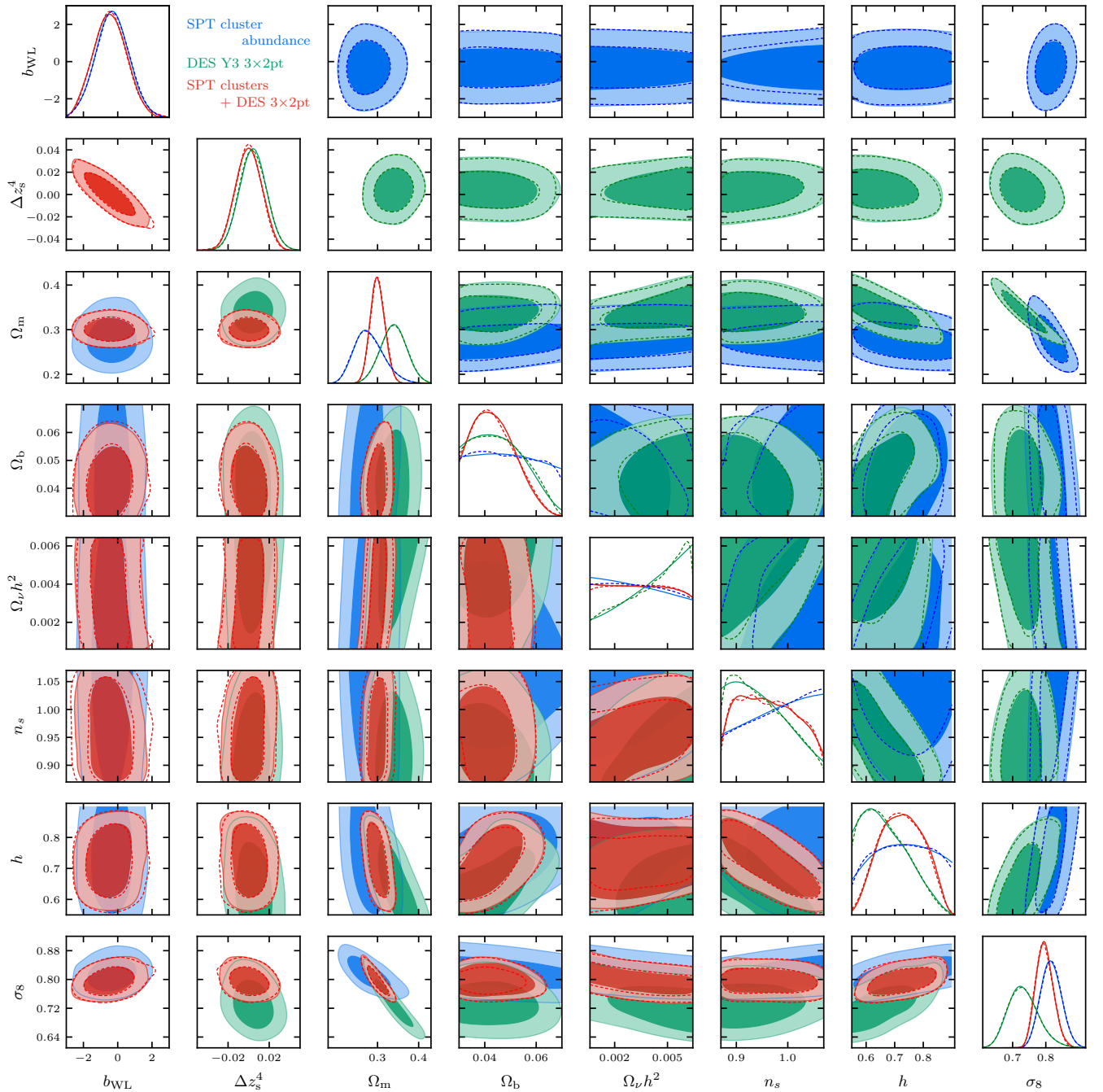


FIG. 6. Parameter constraints (68% and 95% credibility) in Λ CDM. *Upper right triangle*: The original SPT and DES analyses are shown in solid blue and green, posteriors obtained from the trained normalizing flows are shown with dashed lines. *Lower left triangle*: The fiducial joint analysis, in which the DES posterior is updated with the SPT likelihood, is shown with solid red lines; the inverse analysis (SPT posterior updated with DES likelihood) is shown in red dashed lines.

- Oliveira, J. Annis, S. Avila, et al., Phys. Rev. D **105**, 023520 (2022), [arXiv:2105.13549](https://arxiv.org/abs/2105.13549).
- [8] S. More, S. Sugiyama, H. Miyatake, M. M. Rau, M. Shirasaki, X. Li, A. J. Nishizawa, K. Osato, T. Zhang, M. Takada, et al., Phys. Rev. D **108**, 123520 (2023), [arXiv:2304.00703](https://arxiv.org/abs/2304.00703).
- [9] H. Miyatake, S. Sugiyama, M. Takada, T. Nishimichi, X. Li, M. Shirasaki, S. More, Y. Kobayashi, A. J. Nishizawa, M. M. Rau, et al., Phys. Rev. D **108**, 123517 (2023), [arXiv:2304.00704](https://arxiv.org/abs/2304.00704).
- [10] S. Sugiyama, H. Miyatake, S. More, X. Li, M. Shirasaki, M. Takada, Y. Kobayashi, R. Takahashi, T. Nishimichi, A. J. Nishizawa, et al., Phys. Rev. D **108**, 123521 (2023),

- arXiv:2304.00705.
- [11] R. A. Sunyaev and Y. B. Zeldovich, *Comments on Astrophysics and Space Physics* **4**, 173 (1972).
- [12] Z. Staniszewski, P. A. R. Ade, K. A. Aird, B. A. Benson, L. E. Bleem, J. E. Carlstrom, C. L. Chang, H. M. Cho, T. M. Crawford, A. T. Crites, et al., *ApJ* **701**, 32 (2009), arXiv:0810.1578.
- [13] L. E. Bleem, B. Stalder, T. de Haan, K. A. Aird, S. W. Allen, D. E. Applegate, M. L. N. Ashby, M. Bautz, M. Bayliss, B. A. Benson, et al., *ApJS* **216**, 27 (2015), arXiv:1409.0850.
- [14] Planck Collaboration, P. A. R. Ade, N. Aghanim, M. Arnaud, M. Ashdown, J. Aumont, C. Baccigalupi, A. J. Banday, R. B. Barreiro, R. Barrera, et al., *A&A* **594**, A27 (2016), arXiv:1502.01598.
- [15] M. Hilton, C. Sifón, S. Naess, M. Madhavacheril, M. Oguri, E. Rozo, E. Rykoff, T. M. C. Abbott, S. Adhikari, M. Agüena, et al., *ApJS* **253**, 3 (2021), arXiv:2009.11043.
- [16] L. E. Bleem, M. Klein, T. M. C. Abbot, P. A. R. Ade, M. Agüena, O. Alves, A. J. Anderson, F. Andrade-Oliveira, B. Ansarinejad, M. Archipley, et al., *The Open Journal of Astrophysics* **7**, 13 (2024), arXiv:2311.07512.
- [17] M. Klein, J. J. Mohr, and C. T. Davies, *A&A* **690**, A322 (2024), arXiv:2406.14754.
- [18] Í. Zubeldia, J.-B. Melin, J. Chluba, and R. Battye (2024), arXiv:2408.06189.
- [19] J. E. Carlstrom, P. A. R. Ade, K. A. Aird, B. A. Benson, L. E. Bleem, S. Busetti, C. L. Chang, E. Chauvin, H. M. Cho, T. M. Crawford, et al., *PASP* **123**, 568 (2011), arXiv:0907.4445.
- [20] S. Bocquet, S. Grandis, L. E. Bleem, M. Klein, J. J. Mohr, T. Schrabback, T. M. C. Abbott, P. A. R. Ade, M. Agüena, A. Alarcon, et al., *Phys. Rev. D* **110**, 083510 (2024), arXiv:2401.02075.
- [21] C. To, E. Krause, E. Rozo, H. Wu, D. Gruen, R. H. Wechsler, T. F. Eifler, E. S. Rykoff, M. Costanzi, M. R. Becker, et al., *Phys. Rev. Lett.* **126**, 141301 (2021), arXiv:2010.01138.
- [22] E. S. Rykoff, E. Rozo, M. T. Busha, C. E. Cunha, A. Finoguenov, A. Evrard, J. Hao, B. P. Koester, A. Leauthaud, B. Nord, et al., *ApJ* **785**, 104 (2014), arXiv:1303.3562.
- [23] J. Zuntz, E. Sheldon, S. Samuroff, M. A. Troxel, M. Jarvis, N. MacCrann, D. Gruen, J. Prat, C. Sánchez, A. Choi, et al., *MNRAS* **481**, 1149 (2018), arXiv:1708.01533.
- [24] B. Hoyle, D. Gruen, G. M. Bernstein, M. M. Rau, J. De Vicente, W. G. Hartley, E. Gaztanaga, J. DeRose, M. A. Troxel, C. Davis, et al., *MNRAS* **478**, 592 (2018), arXiv:1708.01532.
- [25] J. Elvin-Poole, M. Crocce, A. J. Ross, T. Giannantonio, E. Rozo, E. S. Rykoff, S. Avila, N. Banik, J. Blazek, S. L. Bridle, et al., *Phys. Rev. D* **98**, 042006 (2018), arXiv:1708.01536.
- [26] DES Collaboration, T. M. C. Abbott, F. B. Abdalla, A. Alarcon, J. Aleksić, S. Allam, S. Allen, A. Amara, J. Annis, J. Asorey, et al., *Phys. Rev. D* **98**, 043526 (2018), arXiv:1708.01530.
- [27] M. Gatti, E. Sheldon, A. Amon, M. Becker, M. Troxel, A. Choi, C. Doux, N. MacCrann, A. Navarro-Alsina, I. Harrison, et al., *MNRAS* **504**, 4312 (2021), arXiv:2011.03408.
- [28] E. S. Sheldon and E. M. Huff, *ApJ* **841**, 24 (2017), arXiv:1702.02601.
- [29] A. Porredon, M. Crocce, J. Elvin-Poole, R. Cawthon, G. Giannini, J. De Vicente, A. Carnero Rosell, I. Ferrero, E. Krause, X. Fang, et al., *Phys. Rev. D* **106**, 103530 (2022), arXiv:2105.13546.
- [30] C. Sánchez, J. Prat, G. Zacharegkas, S. Pandey, E. Baxter, G. M. Bernstein, J. Blazek, R. Cawthon, C. Chang, E. Krause, et al., *Phys. Rev. D* **105**, 083529 (2022), arXiv:2105.13542.
- [31] R. E. Smith, J. A. Peacock, A. Jenkins, S. D. M. White, C. S. Frenk, F. R. Pearce, P. A. Thomas, G. Efstathiou, and H. M. P. Couchman, *MNRAS* **341**, 1311 (2003), arXiv:astro-ph/0207664.
- [32] R. Takahashi, M. Sato, T. Nishimichi, A. Taruya, and M. Oguri, *ApJ* **761**, 152 (2012), arXiv:1208.2701.
- [33] J. A. Blazek, N. MacCrann, M. A. Troxel, and X. Fang, *Phys. Rev. D* **100**, 103506 (2019), arXiv:1708.09247.
- [34] O. Friedrich, F. Andrade-Oliveira, H. Camacho, O. Alves, R. Rosenfeld, J. Sanchez, X. Fang, T. F. Eifler, E. Krause, C. Chang, et al., *MNRAS* **508**, 3125 (2021), arXiv:2012.08568.
- [35] S. Bocquet, S. Grandis, L. E. Bleem, M. Klein, J. J. Mohr, M. Agüena, A. Alarcon, S. Allam, S. W. Allen, O. Alves, et al., *Phys. Rev. D* **110**, 083509 (2024), arXiv:2310.12213.
- [36] L. E. Bleem, S. Bocquet, B. Stalder, M. D. Gladders, P. A. R. Ade, S. W. Allen, A. J. Anderson, J. Annis, M. L. N. Ashby, J. E. Austermann, et al., *ApJS* **247**, 25 (2020), arXiv:1910.04121.
- [37] M. Klein, J. J. Mohr, S. Desai, H. Israel, S. Allam, A. Benoit-Lévy, D. Brooks, E. Buckley-Geer, A. Carnero Rosell, M. Carrasco Kind, et al., *MNRAS* **474**, 3324 (2018), arXiv:1706.06577.
- [38] M. Klein, J. J. Mohr, S. Bocquet, M. Agüena, S. W. Allen, O. Alves, B. Ansarinejad, M. L. N. Ashby, D. Bacon, M. Bayliss, et al., *MNRAS* **531**, 3973 (2024), arXiv:2309.09908.
- [39] E. L. Wright, P. R. M. Eisenhardt, A. K. Mainzer, M. E. Ressler, R. M. Cutri, T. Jarrett, J. D. Kirkpatrick, D. Padgett, R. S. McMillan, M. Skrutskie, et al., *AJ* **140**, 1868 (2010), arXiv:1008.0031.
- [40] B. Stalder, A. A. Stark, S. M. Amato, J. Geary, S. A. Shectman, C. W. Stubbs, and A. Szentgyorgyi, in *Ground-based and Airborne Instrumentation for Astronomy V*, edited by S. K. Ramsay, I. S. McLean, and H. Takami (2014), vol. 9147 of *Society of Photo-Optical Instrumentation Engineers (SPIE) Conference Series*, p. 91473Y.
- [41] G. G. Fazio, J. L. Hora, L. E. Allen, M. L. N. Ashby, P. Barmby, L. K. Deutsch, J. S. Huang, S. Kleiner, M. Marengo, S. T. Megeath, et al., *ApJS* **154**, 10 (2004), arXiv:astro-ph/0405616.
- [42] T. Schrabback, D. Applegate, J. P. Dietrich, H. Hoekstra, S. Bocquet, A. H. Gonzalez, A. von der Linden, M. McDonald, C. B. Morrison, S. F. Raihan, et al., *MNRAS* **474**, 2635 (2018), arXiv:1611.03866.
- [43] S. F. Raihan, T. Schrabback, H. Hildebrandt, D. Applegate, and G. Mahler, *MNRAS* **497**, 1404 (2020), arXiv:2007.01211.
- [44] B. Hernández-Martín, T. Schrabback, H. Hoekstra, N. Martinet, J. Hlavacek-Larrondo, L. E. Bleem, M. D. Gladders, B. Stalder, A. A. Stark, and M. Bayliss, *A&A* **640**, A117 (2020), arXiv:2007.00386.

- [45] T. Schrabback, S. Bocquet, M. Sommer, H. Zohren, J. L. van den Busch, B. Hernández-Martín, H. Hoekstra, S. F. Raihan, M. Schirmer, D. Applegate, et al., *MNRAS* **505**, 3923 (2021), [arXiv:2009.07591](#).
- [46] H. Zohren, T. Schrabback, S. Bocquet, M. Sommer, F. Raihan, B. Hernández-Martín, O. Marggraf, B. Ansarnejad, M. B. Bayliss, L. E. Bleem, et al., *A&A* **668**, A18 (2022), [arXiv:2208.10232](#).
- [47] S. Grandis, S. Bocquet, J. J. Mohr, M. Klein, and K. Dolag, *MNRAS* **507**, 5671 (2021), [arXiv:2103.16212](#).
- [48] J. Tinker, A. V. Kravtsov, A. Klypin, K. Abazajian, M. Warren, G. Yepes, S. Gottlöber, and D. E. Holz, *ApJ* **688**, 709 (2008), [arXiv:0803.2706](#).
- [49] E. Krause and T. Eifler, *MNRAS* **470**, 2100 (2017), [arXiv:1601.05779](#).
- [50] C.-H. To, E. Krause, E. Rozo, H.-Y. Wu, D. Gruen, J. DeRose, E. Rykoff, R. H. Wechsler, M. Becker, M. Costanzi, et al., *MNRAS* **502**, 4093 (2021), [arXiv:2008.10757](#).
- [51] J. Myles, A. Alarcon, A. Amon, C. Sánchez, S. Everett, J. DeRose, J. McCullough, D. Gruen, G. M. Bernstein, M. A. Troxel, et al., *MNRAS* **505**, 4249 (2021), [arXiv:2012.08566](#).
- [52] N. MacCrann, M. R. Becker, J. McCullough, A. Amon, D. Gruen, M. Jarvis, A. Choi, M. A. Troxel, E. Sheldon, B. Yanny, et al., *MNRAS* **509**, 3371 (2022), [arXiv:2012.08567](#).
- [53] D. Jimenez Rezende and S. Mohamed (2015), [arXiv:1505.05770](#).
- [54] I. Kobzyev, S. J. D. Prince, and M. A. Brubaker (2019), [arXiv:1908.09257](#).
- [55] G. Papamakarios, T. Pavlakou, and I. Murray (2017), [arXiv:1705.07057](#).
- [56] C. Doux, E. Baxter, P. Lemos, C. Chang, A. Alarcon, A. Amon, A. Campos, A. Choi, M. Gatti, D. Gruen, et al., *MNRAS* **503**, 2688 (2021), [arXiv:2011.03410](#).
- [57] S. Navas, C. Amsler, T. Gutsche, C. Hanhart, J. J. Hernández-Rey, C. Lourenço, A. Masoni, M. Mikhasenko, R. E. Mitchell, C. Patrignani, et al. (Particle Data Group Collaboration), *Phys. Rev. D* **110**, 030001 (2024).
- [58] Planck Collaboration, N. Aghanim, Y. Akrami, M. Ashdown, J. Aumont, C. Baccigalupi, M. Ballardini, A. J. Banday, R. B. Barreiro, N. Bartolo, et al., *A&A* **641**, A6 (2020), [arXiv:1807.06209](#).
- [59] M. S. Madhavacheril, F. J. Qu, B. D. Sherwin, N. MacCrann, Y. Li, I. Abril-Cabezas, P. A. R. Ade, S. Aiola, T. Alford, M. Amiri, et al., *ApJ* **962**, 113 (2024), [arXiv:2304.05203](#).
- [60] F. J. Qu, B. D. Sherwin, M. S. Madhavacheril, D. Han, K. T. Crowley, I. Abril-Cabezas, P. A. R. Ade, S. Aiola, T. Alford, M. Amiri, et al., *ApJ* **962**, 112 (2024), [arXiv:2304.05202](#).
- [61] DES and SPT Collaborations, T. M. C. Abbott, M. Aguena, A. Alarcon, O. Alves, A. Amon, F. Andrade-Oliveira, J. Annis, B. Ansarnejad, S. Avila, et al., *Phys. Rev. D* **107**, 023531 (2023), [arXiv:2206.10824](#).
- [62] V. Ghirardini, E. Bulbul, E. Artis, N. Clerc, C. Garrel, S. Grandis, M. Kluge, A. Liu, Y. E. Bahar, F. Balzer, et al., *A&A* **689**, A298 (2024), [arXiv:2402.08458](#).
- [63] S. Grandis, V. Ghirardini, S. Bocquet, C. Garrel, J. J. Mohr, A. Liu, M. Kluge, L. Kimmig, T. H. Reiprich, A. Alarcon, et al., *A&A* **687**, A178 (2024), [arXiv:2402.08455](#).
- [64] DESI Collaboration, A. G. Adame, J. Aguilar, S. Ahlen, S. Alam, D. M. Alexander, M. Alvarez, O. Alves, A. Anand, U. Andrade, et al. (2024), [arXiv:2404.03002](#).
- [65] M. Loverde and Z. J. Weiner, *arXiv e-prints* [arXiv:2410.00090](#) (2024), [arXiv:2410.00090](#).
- [66] DES Collaboration, T. M. C. Abbott, M. Aguena, A. Alarcon, O. Alves, A. Amon, F. Andrade-Oliveira, J. Annis, S. Avila, D. Bacon, et al., *Phys. Rev. D* **107**, 083504 (2023), [arXiv:2207.05766](#).
- [67] DES Collaboration, T. M. C. Abbott, M. Acevedo, M. Aguena, A. Alarcon, S. Allam, O. Alves, A. Amon, F. Andrade-Oliveira, J. Annis, et al., *ApJ* **973**, L14 (2024).
- [68] D. Brout, D. Scolnic, B. Popovic, A. G. Riess, A. Carr, J. Zuntz, R. Kessler, T. M. Davis, S. Hinton, D. Jones, et al., *ApJ* **938**, 110 (2022), [arXiv:2202.04077](#).
- [69] D. Rubin, G. Aldering, M. Betoule, A. Fruchter, X. Huang, A. G. Kim, C. Lidman, E. Linder, S. Perlmutter, P. Ruiz-Lapuente, et al. (2023), [arXiv:2311.12098](#).
- [70] J. A. Sobrin, A. J. Anderson, A. N. Bender, B. A. Benson, D. Dutcher, A. Foster, N. Goekner-Wald, J. Montgomery, A. Nadolski, A. Rahlin, et al., *ApJS* **258**, 42 (2022), [arXiv:2106.11202](#).
- [71] SO Collaboration, P. Ade, J. Aguirre, Z. Ahmed, S. Aiola, A. Ali, D. Alonso, M. A. Alvarez, K. Arnold, P. Ashton, et al., *J. Cosmology Astropart. Phys.* **2019**, 056 (2019), [arXiv:1808.07445](#).
- [72] CMB-S4 Collaboration, K. N. Abazajian, P. Adshead, Z. Ahmed, S. W. Allen, D. Alonso, K. S. Arnold, C. Baccigalupi, J. G. Bartlett, N. Battaglia, et al. (2016), [arXiv:1610.02743](#).
- [73] R. Laureijs, J. Amiaux, S. Arduini, J. L. Auguères, J. Brinchmann, R. Cole, M. Cropper, C. Dabin, L. Duval, A. Ealet, et al. (2011), [arXiv:1110.3193](#).
- [74] Euclid Collaboration, Y. Mellier, Abdurro'uf, J. A. Acevedo Barroso, A. Achúcarro, J. Adamek, R. Adam, G. E. Addison, N. Aghanim, M. Aguena, et al. (2024), [arXiv:2405.13491](#).
- [75] LSST Science Collaboration, P. A. Abell, J. Allison, S. F. Anderson, J. R. Andrew, J. R. P. Angel, L. Armus, D. Arnett, S. J. Asztalos, T. S. Axelrod, et al. (2009), [arXiv:0912.0201](#).
- [76] F. Ge, M. Millea, E. Camphuis, C. Daley, N. Huang, Y. Omori, W. Quan, E. Anderes, A. J. Anderson, B. Ansarnejad, et al. (2024), [arXiv:2411.06000](#).

AFFILIATIONS

¹ University Observatory, Faculty of Physics, Ludwig-Maximilians-Universität, Scheinerstr. 1, 81679 Munich, Germany

² Universität Innsbruck, Institut für Astro- und Teilchenphysik, Technikerstr. 25/8, 6020 Innsbruck, Austria

³ Department of Astronomy/Steward Observatory, University of Arizona, 933 North Cherry Avenue, Tucson, AZ 85721-0065, USA

⁴ Center for Cosmology and Astro-Particle Physics, The Ohio State University, Columbus, OH 43210, USA

⁵ Department of Astronomy and Astrophysics, University of Chicago, Chicago, IL 60637, USA

⁶ Kavli Institute for Cosmological Physics, University of

Chicago, 5640 South Ellis Avenue, Chicago, IL 60637, USA

⁷ High-Energy Physics Division, Argonne National Laboratory, 9700 South Cass Avenue, Lemont, IL 60439, USA

⁸ Max Planck Institute for Extraterrestrial Physics, Gießenbachstr. 1, 85748 Garching, Germany

⁹ Argelander-Institut für Astronomie, Auf dem Hügel 71, 53121 Bonn, Germany

¹⁰ Institute of Space Sciences (ICE, CSIC), Campus UAB, Carrer de Can Magrans, s/n, 08193 Barcelona, Spain

¹¹ Department of Physics, University of Michigan, Ann Arbor, MI 48109, USA

¹² Department of Astrophysical Sciences, Princeton University, Peyton Hall, Princeton, NJ 08544, USA

¹³ Institute for Astronomy, University of Hawai'i, 2680 Woodlawn Drive, Honolulu, HI 96822, USA

¹⁴ Physics Department, 2320 Chamberlin Hall, University of Wisconsin-Madison, 1150 University Avenue Madison, WI 53706-1390, USA

¹⁵ Department of Physics and Astronomy, University of Pennsylvania, Philadelphia, PA 19104, USA

¹⁶ Department of Physics, Northeastern University, Boston, MA 02115, USA

¹⁷ Brookhaven National Laboratory, Bldg 510, Upton, NY 11973, USA

¹⁸ Instituto de Física Teórica, Universidade Estadual Paulista, São Paulo, Brazil

¹⁹ Laboratório Interinstitucional de e-Astronomia - LIneA, Rua Gal. José Cristino 77, Rio de Janeiro, RJ - 20921-400, Brazil

²⁰ Department of Physics, Carnegie Mellon University, Pittsburgh, Pennsylvania 15312, USA

²¹ NSF AI Planning Institute for Physics of the Future, Carnegie Mellon University, Pittsburgh, PA 15213, USA

²² Instituto de Astrofísica de Canarias, E-38205 La Laguna, Tenerife, Spain

²³ Universidad de La Laguna, Dpto. Astrofísica, E-38206 La Laguna, Tenerife, Spain

²⁴ Center for Astrophysical Surveys, National Center for Supercomputing Applications, 1205 West Clark St., Urbana, IL 61801, USA

²⁵ Department of Astronomy, University of Illinois Urbana-Champaign, 1002 W. Green Street, Urbana, IL 61801, USA

²⁶ Physics Department, William Jewell College, Liberty, MO 64068, USA

²⁷ Department of Physics, Duke University Durham, NC 27708, USA

²⁸ NASA Goddard Space Flight Center, 8800 Greenbelt Rd, Greenbelt, MD 20771, USA

²⁹ Jodrell Bank Center for Astrophysics, School of Physics and Astronomy, University of Manchester, Oxford Road, Manchester, M13 9PL, UK

³⁰ Institut d'Estudis Espacials de Catalunya (IEEC), 08034 Barcelona, Spain

³¹ Kavli Institute for Particle Astrophysics and Cosmol-

ogy, P. O. Box 2450, Stanford University, Stanford, CA 94305, USA

³² Lawrence Berkeley National Laboratory, 1 Cyclotron Road, Berkeley, CA 94720, USA

³³ Fermi National Accelerator Laboratory, P.O. Box 500, Batavia, IL 60510, USA

³⁴ Université Grenoble Alpes, CNRS, LPSC-IN2P3, 38000 Grenoble, France

³⁵ Jet Propulsion Laboratory, California Institute of Technology, 4800 Oak Grove Dr., Pasadena, CA 91109, USA

³⁶ Department of Physics & Astronomy, University College London, Gower Street, London, WC1E 6BT, UK

³⁷ Department of Physics and Astronomy, University of Waterloo, 200 University Ave W, Waterloo, ON N2L 3G1, Canada

³⁸ California Institute of Technology, 1200 East California Boulevard, Pasadena, CA 91125, USA

³⁹ Department of Astronomy, University of California, Berkeley, 501 Campbell Hall, Berkeley, CA 94720, USA

⁴⁰ SLAC National Accelerator Laboratory, Menlo Park, CA 94025, USA

⁴¹ Kavli Institute for Cosmology, University of Cambridge, Madingley Road, Cambridge CB3 0HA, UK

⁴² Institut de Física d'Altes Energies (IFAE), The Barcelona Institute of Science and Technology, Campus UAB, 08193 Bellaterra (Barcelona) Spain

⁴³ School of Physics and Astronomy, Cardiff University, CF24 3AA, UK

⁴⁴ Department of Astronomy, University of Geneva, ch. d'Écogia 16, CH-1290 Versoix, Switzerland

⁴⁵ Department of Physics, University of Arizona, Tucson, AZ 85721, USA

⁴⁶ Department of Physics and Astronomy, Pevensey Building, University of Sussex, Brighton, BN1 9QH, UK

⁴⁷ Instituto de Astrofísica e Ciências do Espaço, Faculdade de Ciências, Universidade de Lisboa, 1769-016 Lisboa, Portugal

⁴⁸ Department of Applied Mathematics and Theoretical Physics, University of Cambridge, Cambridge CB3 0WA, UK

⁴⁹ Perimeter Institute for Theoretical Physics, 31 Caroline St. North, Waterloo, ON N2L 2Y5, Canada

⁵⁰ Instituto de Física Gleb Wataghin, Universidade Estadual de Campinas, 13083-859, Campinas, SP, Brazil

⁵¹ Kavli Institute for the Physics and Mathematics of the Universe (WPI), UTIAS, The University of Tokyo, Kashiwa, Chiba 277-8583, Japan

⁵² Centro de Investigaciones Energéticas, Medioambientales y Tecnológicas (CIEMAT), Madrid, Spain

⁵³ Ruhr University Bochum, Faculty of Physics and Astronomy, Astronomical Institute, German Centre for Cosmological Lensing, 44780 Bochum, Germany

⁵⁴ Nordita, KTH Royal Institute of Technology and Stockholm University, Hannes Alfvéns väg 12, SE-10691 Stockholm, Sweden

⁵⁵ Department of Physics, University of Genova and

INFN, Via Dodecaneso 33, 16146, Genova, Italy

⁵⁶ ICTP South American Institute for Fundamental Research | Instituto de Física Teórica, Universidade Estadual Paulista, São Paulo, Brazil

⁵⁷ Space Telescope Science Institute, 3700 San Martin Drive, Baltimore, MD 21218, USA

⁵⁸ Department of Physics and Astronomy, Stony Brook University, Stony Brook, NY 11794, USA

⁵⁹ Institut de Recherche en Astrophysique et Planétologie (IRAP), Université de Toulouse, CNRS, UPS, CNES, 14 Av. Edouard Belin, 31400 Toulouse, France

⁶⁰ Excellence Cluster Origins, Boltzmannstr. 2, 85748 Garching, Germany

⁶¹ Department of Physics, Stanford University, 382 Via Pueblo Mall, Stanford, CA 94305, USA

⁶² Department of Physics, Southern Methodist University, Dallas, TX 75205, USA

⁶³ Cerro Tololo Inter-American Observatory, NSF's National Optical-Infrared Astronomy Research Laboratory, Casilla 603, La Serena, Chile

⁶⁴ Institute for Astronomy, University of Edinburgh, Edinburgh EH9 3HJ, UK

⁶⁵ School of Physics and Astronomy, Cardiff University, Cardiff CF24 3YB, United Kingdom

⁶⁶ Kavli Institute for Particle Astrophysics and Cosmology, Stanford University, 452 Lomita Mall, Stanford, CA 94305, USA

⁶⁷ SLAC National Accelerator Laboratory, 2575 Sand Hill Road, Menlo Park, CA 94025, USA

⁶⁸ School of Physics, University of Melbourne, Parkville, VIC 3010, Australia

⁶⁹ NIST Quantum Devices Group, 325 Broadway Mail-code 817.03, Boulder, CO 80305, USA

⁷⁰ Department of Physics, University of Colorado, Boulder, CO 80309, USA

⁷¹ Department of Physics, University of Cincinnati, Cincinnati, OH 45221, USA

⁷² Department of Astronomy and Astrophysics, University of Chicago, 5640 South Ellis Avenue, Chicago, IL 60637, USA

⁷³ Department of Physics and Astronomy, University of Missouri, 5110 Rockhill Road, Kansas City, MO 64110, USA

⁷⁴ Enrico Fermi Institute, University of Chicago, 5640 South Ellis Avenue, Chicago, IL 60637, USA

⁷⁵ Institute of Cosmology & Gravitation, University of Portsmouth, Dennis Sciama Building, Portsmouth, PO1 3FX, UK

⁷⁶ Department of Physics, University of Chicago, 5640 South Ellis Avenue, Chicago, IL 60637, USA

⁷⁷ Department of Physics and McGill Space Institute, McGill University, 3600 Rue University, Montreal, Quebec H3A 2T8, Canada

⁷⁸ School of Mathematics, Statistics & Computer Science, University of KwaZulu-Natal, Durban, South Africa

⁷⁹ University of Chicago, 5640 South Ellis Avenue, Chicago, IL 60637, USA

⁸⁰ Jet Propulsion Laboratory, California Institute of Technology, Pasadena, CA 91011, USA

⁸¹ Astronomy Unit, Department of Physics, University of Trieste, via Tiepolo 11, I-34131 Trieste, Italy

⁸² INAF-Osservatorio Astronomico di Trieste, via G. B. Tiepolo 11, I-34143 Trieste, Italy

⁸³ Institute for Fundamental Physics of the Universe, Via Beirut 2, 34014 Trieste, Italy

⁸⁴ Cornell University, Ithaca, NY 14853, USA

⁸⁵ Hamburger Sternwarte, Universität Hamburg, Gojenbergsweg 112, 21029 Hamburg, Germany

⁸⁶ School of Mathematics and Physics, University of Queensland, Brisbane, QLD 4072, Australia

⁸⁷ Institute of Particle and Nuclear Studies (IPNS), High Energy Accelerator Research Organization (KEK), Tsukuba, Ibaraki 305-0801, Japan

⁸⁸ International Center for Quantum-field Measurement Systems for Studies of the Universe and Particles (QUP), High Energy Accelerator Research Organization (KEK), Tsukuba, Ibaraki 305-0801, Japan

⁸⁹ Canadian Institute for Advanced Research, CIFAR Program in Gravity and the Extreme Universe, Toronto, ON, M5G 1Z8, Canada

⁹⁰ Department of Astrophysical and Planetary Sciences, University of Colorado, Boulder, CO 80309, USA

⁹¹ Departments of Statistics and Data Sciences, University of Texas at Austin, Austin, TX 78757, USA

⁹² NSF-Simons AI Institute for Cosmic Origins, University of Texas at Austin, Austin, TX 78757, USA

⁹³ Institute of Cosmology and Gravitation, University of Portsmouth, Dennis Sciama Building, Burnaby Road, Portsmouth, PO1 3FX, UK

⁹⁴ Harvey Mudd College, 301 Platt Boulevard, Claremont, CA 91711, USA

⁹⁵ Institute of Cosmology and Gravitation, University of Portsmouth, Portsmouth, PO1 3FX, UK

⁹⁶ Institute of Space Sciences (ICE, CSIC), Campus UAB, Carrer de Can Magrans, s/n, 08193 Barcelona, Spain

⁹⁷ European Southern Observatory, Karl-Schwarzschild-Str., DE-85748 Garching b. München, Germany

⁹⁸ CSIRO Space & Astronomy, PO Box 1130, Bentley WA 6102, Australia

⁹⁹ Département de Physique, Université de Montréal, Succ. Centre-Ville, Montréal, Québec, H3C 3J7, Canada

¹⁰⁰ Department of Physics, University of Illinois Urbana-Champaign, 1110 W. Green Street, Urbana, IL 61801, USA

¹⁰¹ Santa Cruz Institute for Particle Physics, Santa Cruz, CA 95064, USA

¹⁰² Department of Physics, University of California, Berkeley, CA 94720, USA

¹⁰³ Center for Astrophysics | Harvard & Smithsonian, 60 Garden Street, Cambridge, MA 02138, USA

¹⁰⁴ Department of Physics, University of California, One Shields Avenue, Davis, CA 95616, USA

¹⁰⁵ Australian Astronomical Optics, Macquarie University, North Ryde, NSW 2113, Australia

- ¹⁰⁶ Lowell Observatory, 1400 Mars Hill Rd, Flagstaff, AZ 86001, USA
- ¹⁰⁷ Physics Division, Lawrence Berkeley National Laboratory, Berkeley, CA 94720, USA
- ¹⁰⁸ Centre for Gravitational Astrophysics, College of Science, The Australian National University, ACT 2601, Australia
- ¹⁰⁹ The Research School of Astronomy and Astrophysics, Australian National University, ACT 2601, Australia
- ¹¹⁰ Departamento de Física Matemática, Instituto de Física, Universidade de São Paulo, CP 66318, São Paulo, SP, 05314-970, Brazil
- ¹¹¹ Centre for Extragalactic Astronomy, Durham University, South Road, Durham DH1 3LE, UK
- ¹¹² Institute for Computational Cosmology, Durham University, South Road, Durham DH1 3LE, UK
- ¹¹³ George P. and Cynthia Woods Mitchell Institute for Fundamental Physics and Astronomy, and Department of Physics and Astronomy, Texas A&M University, College Station, TX 77843, USA
- ¹¹⁴ Kavli Institute for Astrophysics and Space Research, Massachusetts Institute of Technology, 77 Massachusetts Avenue, Cambridge, MA 02139, USA
- ¹¹⁵ LPSC Grenoble - 53, Avenue des Martyrs 38026 Grenoble, France
- ¹¹⁶ Institució Catalana de Recerca i Estudis Avançats, E-08010 Barcelona, Spain
- ¹¹⁷ Dunlap Institute for Astronomy & Astrophysics, University of Toronto, 50 St. George Street, Toronto, ON, M5S 3H4, Canada
- ¹¹⁸ David A. Dunlap Department of Astronomy & Astrophysics, University of Toronto, 50 St. George Street, Toronto, ON, M5S 3H4, Canada
- ¹¹⁹ Materials Sciences Division, Argonne National Laboratory, 9700 South Cass Avenue, Lemont, IL 60439, USA
- ¹²⁰ Observatório Nacional, Rua Gal. José Cristino 77, Rio de Janeiro, RJ - 20921-400, Brazil
- ¹²¹ School of Physics and Astronomy, University of Minnesota, 116 Church Street SE Minneapolis, MN 55455, USA
- ¹²² Department of Physics, Case Western Reserve University, Cleveland, OH 44106, USA
- ¹²³ Brookhaven National Laboratory, Upton, NY 11973, USA
- ¹²⁴ Université Paris-Saclay, CNRS, Institut d'Astrophysique Spatiale, 91405, Orsay, France
- ¹²⁵ INAF - Osservatorio Astronomico di Trieste, via G. B. Tiepolo 11, 34143 Trieste, Italy
- ¹²⁶ IFPU - Institute for Fundamental Physics of the Universe, Via Beirut 2, 34014 Trieste, Italy
- ¹²⁷ Instituto de Física, UFRGS, Caixa Postal 15051, Porto Alegre, RS - 91501-970, Brazil
- ¹²⁸ Astronomy Unit, Department of Physics, University of Trieste, via Tiepolo 11, 34131 Trieste, Italy
- ¹²⁹ INFN - National Institute for Nuclear Physics, Via Valerio 2, I-34127 Trieste, Italy
- ¹³⁰ ICSC - Italian Research Center on High Performance Computing, Big Data and Quantum Computing, Italy
- ¹³¹ Liberal Arts Department, School of the Art Institute of Chicago, 112 South Michigan Avenue, Chicago, IL 60603, USA
- ¹³² Department of Astronomy, University of Michigan, 1085 S. University Ave, Ann Arbor, MI 48109, USA
- ¹³³ Three-Speed Logic, Inc., Victoria, B.C., V8S 3Z5, Canada
- ¹³⁴ Physics Department, Lancaster University, Lancaster, LA1 4YB, UK
- ¹³⁵ Department of Physics, Faculty of Science, Chulalongkorn University, 254 Phayathai Road, Pathumwan, Bangkok 10330, Thailand
- ¹³⁶ Computer Science and Mathematics Division, Oak Ridge National Laboratory, Oak Ridge, TN 37831, USA
- ¹³⁷ Space Science and Engineering Division, Southwest Research Institute, San Antonio, TX 78238, USA
- ¹³⁸ Department of Physics and Astronomy, Michigan State University, East Lansing, MI 48824, USA
- ¹³⁹ Department of Astronomy & Astrophysics, University of Toronto, 50 St George St, Toronto, ON, M5S 3H4, Canada